# Corticospinal Controller for Assistive Robot Platform for a 3D application

By

Dhruv Patel

August 2023

A Master's Project submitted to

The Graduate School of the University at Buffalo, The State University of New York

in partial fulfillment of the requirements for the degree of

Master of Science in Engineering Science – Robotics

Department of Mechanical and Aerospace Engineering

# Acknowledgments

I would like to express my deepest gratitude to Dr. Filip Stefanovic of the Department of Biomedical Engineering at the University at Buffalo, who has been a source of guidance and inspiration throughout this research journey. His invaluable feedback and unwavering support have been instrumental in shaping this paper. His constructive suggestions and insights have greatly enhanced the quality of this work.

I am grateful to the COMMAND Lab for providing the resources and environment necessary to conduct this research.

Lastly, I owe a debt of gratitude to my parents, sister, and friends for their unwavering encouragement, patience, and belief in me throughout this endeavor. Their unrelenting support throughout my years of study and through the process of researching and writing this project. This accomplishment would not have been possible without them. I dedicate this work to them. Thank you.

Author

Dhruv Patel

# Abstract

The corticospinal controller is a neural structure inside a human body that carries movement-related information, like hand movement, target selection, muscle coordination, etc. This information is carried from the brain to the spinal cord and undergoes processing based on sensory information. Most upper limb prosthetics and assistive robot limbs are focused on motor control development in the brain rather than the spinal cord and corticospinal tract. However, previous studies have shown a simplified spinal-like biomimetic controller which can be used for goal-oriented reaching tasks in 2 dimensions using varying levels of antagonistic muscle co-contractions (Biceps/Triceps and Extensor/Flexor). The research presented herein provides an alternative approach to intricate 3D motor planning. The current investigation takes an innovative step by broadening this model into a 3D corticospinal tract controller, incorporating an additional set of antagonistic muscles, the Adductor/Abductor, thus enhancing the degree of freedom and intricacy. Through this study, we get a 3-dimensional model to achieve a higher degree of freedom which can extend the use of such a model in complex biomedical rehabilitation devices and assistive robot platforms. The study uses virtual muscle models in Simulink to enable complex and more accurate limb motion in a multi-muscle, multi-joint limb model. The revised model encapsulates a two-link simulated robotic arm equipped for executing diverse reaching maneuvers in a 3D environment. The results of this study we pioneered the unveiling of the CSC model, a sophisticated design tailored for orchestrating 3D motion patterns and trajectory schematics—a dimension not traversed in preceding controller-centric research. Our empirical demonstrations elucidate its dexterity in orchestrating multi-joint robotic arm navigations toward designated objectives. Such augmentation paves the way for an expansive spectrum of movement and has wide-ranging implications in the development of complex biomedical rehabilitative apparatuses and assistive robotic mechanisms.

# Contents

Acknowledgments ..... 2
Abstract ..... 3
List of Figures ..... 5
1 Intro ..... 6
1.1 Purpose of this study ..... 8
1.2 Joint Mechanics ..... 10
1.3 Muscle ..... 11
1.4 Muscle Model ..... 12
1.5 The Virtual Muscle Models. ..... 13
1.6 Trajectory Planning ..... 16
2 Common Engineering Controllers ..... 17
2.1 PID control ..... 17
2.2 Neuro-fuzzy regulator ..... 18
2.3 Model Predictive Controller ..... 19
3 Biomechanical Modeling ..... 20
4 Planning for a 3D Controller ..... 25
4.1 Virtual Muscles ..... 26
5 Creating the Controller ..... 26
6 Experimental Procedures ..... 28
7 Results ..... 30
8 Discussion ..... 34
9 Conclusion ..... 35
10 References ..... 37
11 Appendix A ..... 40

# List of Figures

Figure 1. The ASC. ..... 7

Figure 2. A visual representation of the BuildMuscles function is depicted. ..... 15

Figure 3. Trajectory Planning using Feedback control used in the model. ..... 17

Figure 4. Free Body diagram of robot ..... 21

Figure 5. Frame assignment for Kinematic Analysis ..... 22

Figure 6. Basic Planned Model of the controller used to Design the Simulink Model ..... 25

Figure 7.MATLAB Simulink Model for 3D Corticospinal Controller..... 28

Figure 8. Angle plot of all 3-Muscle pair with respect to time ..... 31

Figure 9.Angle plot of all 3-Muscle pair with respect to time ..... 31

Figure 10.Muscle Force Plot of all 3-Muscle pair with respect to time ..... 33

# 1 Intro

The corticospinal tract controller, an intricate neural system within the human body, oversees a multitude of movement-related functions, including but not limited to hand motion, writing, target selection, and muscle synchronization, by conveying signals from the cerebral cortex to the spinal cord. Recent progress in the domain of upper limb prosthetics and assistive robotics has predominantly focused on cerebral motor control, yet the exploration of spinal cord-based methodologies is emerging.

Earlier research has laid the groundwork by unveiling a streamlined spinal-like biomimetic controller that is adept at performing 2D, goal-directed reaching activities, utilizing antagonistic muscular co-contractions such as those found in Biceps/Triceps and Extensor/Flexor pairs. The study reveals the spinal cord as more than a mere relay between the brain and muscles. Instead, it's a sophisticated neural network, capable of processing sensory data and producing corresponding motor responses. The indirect pathway, incorporating subcortical or spinal intraneuronal systems, plays a key role in feeding information to the motor neurons (Mn) overseeing the forelimbs. This underscores the spinal cord's pivotal role in motion regulation, independently of the brain. Computational modeling of these neurons poses challenges, stemming from the tension between representing biological accuracy and ensuring computational efficiency, especially in expansive neuronal models like the spinal cord.

The Adaptive Spinal Controller (ASC) (developed by Stefanovic, F., & Galiana, H. L. (2014). An adaptive spinal-like controller: tunable biomimetic behavior for a robotic limb. *BioMedical Engineering OnLine*, 13, 151) computes the hand-target error, translating it geometrically to shoulder and elbow motoneurons. In each Mn, this error melds with expected motor outcomes and interneuron (IN) signals, promoting the co-activation of opposing muscles. The incorporated efference copies have a 40ms delay, feeding back sensory discrepancies as anticipated MT force outputs, refining the motor command over discrete time

intervals. The INs facilitate parts' interaction, enhancing joint control. Their co-activation varies between full and none, with the amalgamation of normalized inputs determining MT unit activation levels.

Upon activation, the Virtual Muscle (VM) delivers a force output, updating the MT length for every muscle group. This informs about joint angles, speeds, and more, making it straightforward to ascertain the revised hand position, even in the absence of visual data. Perturbations are also integrable into the system's biomechanics. Hence, the controller updates its error vector once a spatial target's chosen, surpassing a predetermined threshold.

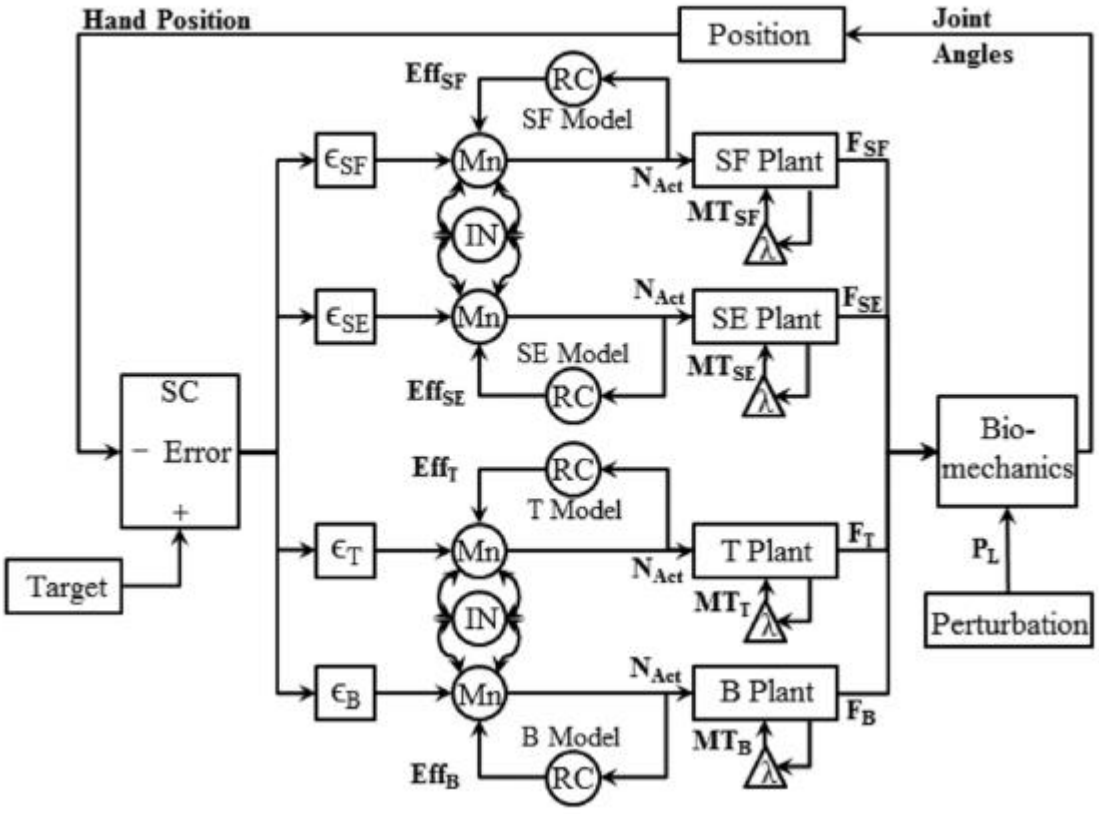


*Figure 1. The ASC. Hand-target errors are projected from the SC as input commands to the controller for each muscle group. The projected error to each muscle group is combined with an efference copy from RCs and a co-activation from the antagonist to produce a muscle activation that drives the joint motion. Normalized activation is the input for the muscle plants and models as required by the VM software. Also, the musculo-tendon lengths (MTi) are the lengths in the muscles and*

*tendons as defined by VM. [Stefanovic, F., & Galiana, H. L. (2014). A simplified spinal-like controller facilitates muscle synergies and robust reaching motions. IEEE Transactions on Neural Systems and Rehabilitation Engineering, 22(1).]*

As shown in the above fig, post-target selection, an error vector, reminiscent of gaze-related reach discharges in the Superior Colliculus, is formed between the hand and target. This is directed to spinal motor centers, potentially initiating a motor response. This error vector is continually adjusted based on the hand's movement, influencing the motor commands in real time. The directive for the shoulder and elbow mirrored as “+” or “-” directions, designates the responsible MT unit, echoing the gain-field traits of error projections in the Superior Colliculus. The generated force from these directives shifts the biomechanics, moving the arm. This cycle continues until the hand-target discrepancy meets a set threshold. The ASC's functioning is visualized in the Simulink platform.

## 1.1 Purpose of this study

Reaching is a fundamental multi-limb motion that allows animals to interact with their environment, including activities like grasping or moving objects. Such motions have consistent characteristics across various species and individuals, such as a direct hand path and synchronized limb movements. Even though reaching might seem straightforward, the underlying systems governing these actions are complex. They involve an extensive neural network encompassing parts of the brain and spinal cord, including the cerebellum, motor cortex, and reflex circuits, among others. This network ensures the coordinated movement of various body parts and muscles.

Researchers have expressed interest in the spinal cord due to its role in sensory-motor interactions. External factors can influence the motor system, implying that the controller for voluntary reaching can respond and integrate external stimuli. Understanding how these motions are coordinated by the brain

and spinal cord is the central issue in motor control. By studying reaching, insights into the neurophysiological system can be gained, which may further inform artificial motion control methods.

The importance of studying reaching controllers lies in the intricate interplay of limb coordination, muscle interaction, sensory-motor integration, and modulation through learning. Achieving a biomimetic controller based on this understanding is challenging, but essential for improving biomedical engineering applications like prosthetics or sensory-based robotics. Developing an effective biomimetic controller for reaching, however, requires careful consideration of various factors, such as comprehensive modeling, broad applicability, and responsiveness to sensory inputs. This is vital to enhance the efficacy and adaptability of rehabilitative devices.

This research underscores the multifaceted nature and computational prowess of spinal motor centers, alluding to inherent intersegmental connections that facilitate intricate motor functions, potentially implicating a central pattern generator (CPG) within the spinal cord. The current investigation takes an innovative step by broadening this model into a 3D corticospinal tract controller, incorporating an additional set of antagonistic muscles, the Adductor/Abductor, thus enhancing the degree of freedom and intricacy. The revised model encapsulates a two-link simulated robotic arm equipped for executing diverse reaching maneuvers in a 3D environment. Such augmentation paves the way for an expansive spectrum of movement and has wide-ranging implications in the development of complex biomedical rehabilitative apparatuses and assistive robotic mechanisms.

The observations mentioned form the basis for our development of a model capable of exhibiting complex motor behaviors. For this conceptual demonstration, we analyze an arm with two joints - the shoulder and the elbow - controlled by a group of six muscle synergies - Shoulder Adductor, Shoulder Abductor, Shoulder Transverse Extensors, Shoulder Transverse Flexors, Biceps, and Triceps. To control the arm's motion via

muscle engagement, we devise an adaptive muscle synergy controller. This controller is grounded in our understanding of reflex circuits housed in the spinal cord.

In this study, we show that the controller can effectively manipulate highly non-linear, biological-like actuators and that it encourages robust behaviors not found in kinematically planned control systems. This achievement is realized by simulating our controller with highly non-linear Virtual Muscles (Cheng, Brown, and Loeb, 2000) that bear a resemblance to those documented in motor control literature. The research presented herein provides an alternative approach to intricate 3D motor planning.

## 1.2 Joint Mechanics

Joint mechanics is the study of how joints, pivotal components of the musculoskeletal system, function and manage forces during movement. Understanding these mechanics is essential for a myriad of applications, from orthopedics and sports medicine to the design of assistive devices.

Human joints are complex assemblies of bones, cartilage, ligaments, tendons, and synovial fluid. They are primarily designed to permit motion and bear loads (Palastanga et al., 2006). The types of joints, including hinge (e.g., elbow) and ball-and-socket (e.g., hip), dictate the nature and range of movement.

Articular cartilage plays a fundamental role in joint mechanics. It reduces friction and distributes loads across the joint (Mow et al., 1992). The health and functionality of this cartilage are essential to avoid degenerative diseases like osteoarthritis.

Joints consist of cartilage, fluids, and connective tissues, each impacting joint function (Hasler et al., 1999; Hasson, Miller, and Caldwell, 2011). Connective tissues determine a joint's position or center of rotation (Debicki and Gribble, 2004) Ligaments and tendons, composed of collagen-rich connective tissue, provide joint stability. Their elasticity and tensile strength properties play a critical role in determining joint mobility and function (Benjamin et al., 2008). The "compliance" or give in a joint, which allows tissues to

stretch or shorten, is an integral feature of preventing injuries during unexpected loads (Hayes & Mockros, 1971; Kearney & Stein, 1997).

Joints are also influenced by "interaction torques," where the movement or force exerted on one joint affects the other due to the interconnectedness of the musculoskeletal system (Bagesteiro & Sainburg, 2002). This dynamic interaction emphasizes the holistic approach required when studying joint mechanics.

Viscous frictional forces in joints, arising from the synovial fluid and changing cartilage geometry, are also pivotal. These forces, combined with rotational mechanics, need intricate consideration in any comprehensive joint model (Ludvig & Kearney, 2007).

To date, numerous biomechanical models have been proposed to simulate joint mechanics. The challenge lies in balancing simplification for computational feasibility and ensuring the model's precision for specific study objectives.

In conclusion, joint mechanics offers insights into the dynamic and intricate nature of human motion. Its study is pivotal in enhancing our understanding of movement, injury prevention, and therapeutic intervention.

## 1.3 Muscle

Muscles are specialized tissues responsible for generating force and facilitating movement in the human body. They play a pivotal role in various physiological and biomechanical processes and can be broadly categorized into three types: skeletal, smooth, and cardiac (Widmaier et al., 2011).

These are composed of slender fiber groupings that, upon contraction, produce motion or force in the connected limbs or sections (Meyer, McCulloch, and Lieber 2011; Hasson, Miller, and Caldwell 2011). Such extrafusal fiber clusters are attached to bones on either side of a joint using tendons. This connection ensures that when compressed, the points where muscles attach draw nearer to each other.

Muscle-tendon connections can either span across a single joint like the knee or multiple joints such as in fingers. Typically, skeletal muscles are arranged in agonist-antagonist pairs like the biceps and triceps. This arrangement facilitates different directional movements. When activated together, they create co-contraction, enhancing posture rigidity (Schmidt, 1978). Muscles' force output is influenced by their length and contraction rate, exhibiting non-linear behavior that's challenging to model (Cheng and Loeb, 2008; Song et al., 2008).

Neural impulses channeled through motor neurons, trigger muscle contractions. Electromyograms (EMGs) have shown that as muscle force increases, motor unit excitation frequency also rises (Schmidt, 1978; Nikitina, 1997). At high frequencies, tetanic contractions can occur, boosting muscle force (Edman and Josephson, 2007). By 125 Hz, muscles achieve a state called 'fused tetanus' (Celichowski and Bichler, 2002), indicating the intricacies of muscle summation.

Some theories propose that signals initiating these contractions may have origins in higher motor regions, including the pre-motor cortex (Ayaz and Chance, 2008). Despite potential CNS-periphery communication delays, the body manages coordinated movements using an array of internal motor system sensors.

## 1.4 Muscle Model

Muscle models are invaluable tools for understanding human motion biomechanics, underpinning developments in rehabilitation, sports science, and robotics. These models delineate the intricate interplay between muscle properties, activation, and resultant forces.

Prominent among these is the Hill-type model, introduced by A.V. Hill in the 1930s. Comprising three components: a contractile element (CE) simulating muscle fibers' force generation, a parallel elastic element (PEE) denoting muscle's passive elasticity when stretched, and a series elastic element (SEE) representing tendon elasticity (Hill, 1938).

Muscle models can be broadly categorized. Phenomenological models, like the Hill-type, illustrate observed behaviors without detailing the physiological processes. Conversely, biophysically based models, such as Huxley's, probe into microscopic muscle contraction processes, particularly the cross-bridge dynamics between actin and myosin (Huxley, 1957).

Recent models incorporate neuromuscular activation dynamics. For example, Lloyd and Buchanan (1996) combined musculotendon dynamics with neural control, offering an integrated perspective of muscle activation.

Accounting for musculotendon properties is crucial since tendons' elasticity can store and release energy, influencing the overall force of the muscle-tendon unit. The significance of tendon properties in muscle function was emphasized by Roberts and Azizi (2011).

A challenge in muscle modeling is the non-linear nature of muscle behavior, as factors like muscle length, contraction velocity, and activation levels intersect, complicating model precision (Cheng and Loeb, 2008; Song et al., 2008).

To conclude, muscle models, with their varying complexities, offer profound insights into muscle function. The choice of a model should correspond with the study goals, balancing complexity against computational needs.

## 1.5 The Virtual Muscle Models.

Virtual muscle models, enabled by computational advancements, offer profound insights into muscle biomechanics. These models strive to replicate the physiological and mechanical properties of muscles, enhancing our understanding of muscle dynamics and their applications in fields like rehabilitation and robotics.

The "Virtual Muscle" software, developed by experts at the University of Southern California (USC), offers a sophisticated tool for simulating and studying the non-linear viscoelastic properties of muscles. Designed for compatibility with MATLAB and Simulink, this software is particularly beneficial for investigating complex muscle models in the context of hierarchical motor control systems. The program effectively maps the association between muscle activation and force, providing a reliable estimation of genuine mammalian muscle behaviors.

Central to these models is Hill's three-element model, which combines a contractile element for active force, a passive elastic element, and a series elastic element (Hill, 1938). Modern models have evolved, incorporating non-linear force-length and force-velocity relationships, which are intrinsic to muscle behavior during diverse activities (Zajac, 1989).

A significant advancement is the integration of neural control strategies in virtual muscle models. For instance, the neuromuscular model by Song et al. (2008) synchronizes motor neuron dynamics with muscle force production, shedding light on muscle control intricacies.

Factoring in fatigue, which alters a muscle's force capacity and dynamics, further enhances the models' realism (Cheng and Loeb, 2008). Proprioceptive feedback, especially from muscle spindles that convey muscle length and rate changes, is now a prominent focus, enriching the models' accuracy in movement representation (Roberts and Azizi, 2011).

These virtual models have vast applications, especially in rehabilitation engineering. They guide prosthetics, assistive devices, and exoskeleton design, highlighting muscle coordination and aiding in post-injury motor function restoration (Lloyd and Buchanan, 1996).

The "Virtual Muscle" model's computational component focuses on deciphering the relationship between activation and force, integrating factors like muscle length, firing rates, and force-velocity dynamics. The

model contemplates parallel elasticities and the "thick filament compression" effect to assess both elastic and contractile dynamics. Muscle force computation is driven by mass and an array of elastic elements.

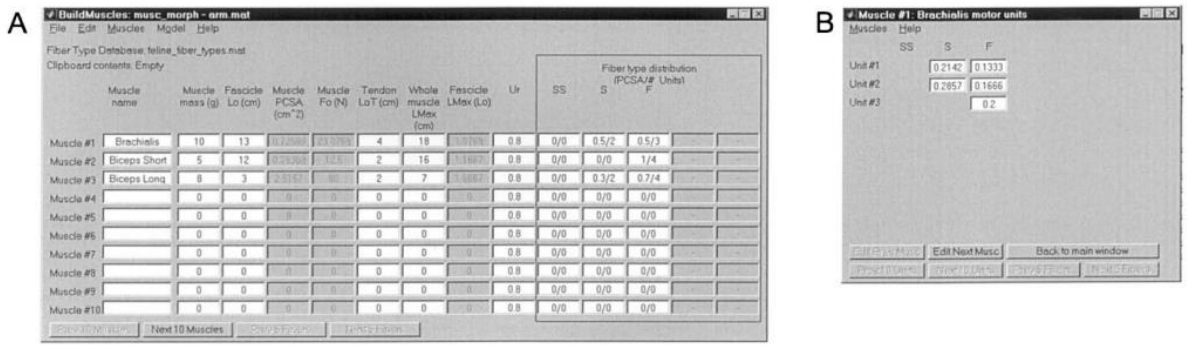


*Figure 2. (A) A visual representation of the BuildMuscles function is depicted. In this primary interface, parameters for every muscle can be adjusted. Individual muscles are enumerated row by row. The left columns are designated for muscle morphometry data, whereas the columns on the right (highlighted with a black border) specify the muscle's fiber type and the count of modeled units. (B) An auxiliary display of the BuildMuscles function showcases and permits edits to the proportional PCSA of every motor unit. Motor units with identical fiber types are organized in columns and are sequentially recruited from the top downwards. (Cheng and Loeb, 2008)*

As shown in the fig above, once the required properties are set, the software crafts a muscle model depicted as a Simulink block. This includes input parameters like muscle and tendon length, normalized activation, and a force-related output. The software suite embodies features that simulate physiological responses, capturing elements like the interplay of length and velocity with force, sequential fiber recruitment, and innate rigidity.

In essence, "Virtual Muscle" offers a niche software tool to simulate muscles' intricate behaviors, elevating motor control systems research. By offering a reliable muscle function portrayal, it becomes an essential resource for testing and affirming new biomimetic controllers in practical scenarios.

To summarize, virtual muscle models merge experimental data with biomechanics, promising a future of comprehensive models replicating intricate muscle functions.

## 1.6 Trajectory Planning

Flash and Hogan, in their 1985 work, put forth a conceptual framework positing that the coordination of arm movements is predicated on predetermined trajectory paths within extracorporeal space. Within this model, trajectories of the hand are computed in advance and subsequently implemented by aligning joint angles to realize the intended trajectory. An intrinsic aspect of this paradigm is the emphasis on maintaining smoothness throughout the motion, facilitated by internal representations within the cerebellum that orchestrate both feed-forward and feedback-control processes.

Empirical validation of this theory has been provided through experiments that have revealed consistent hand trajectories and characteristic bell-shaped speed profiles during the execution of reaching movements. In this context, feedback control serves to contrast actualized trajectories with intended ones, whereas feed-forward control, founded on internal templates, enables the issuance of motor directives without appreciable delays.

Inherent within the trajectory planning model are consistent features including invariant patterns in hand trajectories, synchronized interplay of speed, form, and timing, and its applicability in elucidating control dynamics in activities such as handwriting and navigating around obstacles. Nonetheless, the model is not without its shortcomings, particularly in the integration of external disturbances and adaptive responses to real-time changes during motion.

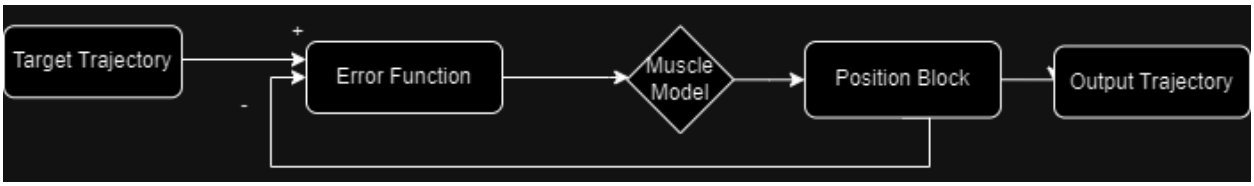


*Figure 3. Trajectory Planning using Feedback control used in the model.*

Though encumbered by certain limitations, the trajectory planning approach has found increasing acceptance within the scientific community, attributable to its underlying advantages and plausible alignment with biological systems. Additional inquiry and methodological refinement are necessary to untangle the intricate aspects of complex arm movements and further enhance the explanatory and predictive power of the model.

# 2 Common Engineering Controllers

Engineering controllers represent specialized devices or systems employed across diverse engineering fields to modulate and govern the dynamics of physical systems or processes. Functionally, these controllers operate by monitoring the existing state of a given system, juxtaposing it with a pre-determined target state, and subsequently formulating control signals to modify the system's inputs or outputs. Through this mechanism, they facilitate the enhancement of system performance and the realization of designated goals. Drawing on prior research, we are employing these controllers as an innovative solution to address the challenges associated with each control problem.

## 2.1 PID control

A PID controller (Proportional-Integral-Derivative controller) is a widely used control system mechanism in industrial control systems. It combines three different constants to compute the control signal, and these constants are tuned to get the desired response from the system. The three components are:

Proportional (P): The proportional term produces an output value that is proportional to the current error value. The proportional response can be adjusted by multiplying the error by a known constant known as $K_p$, the proportional gain constant.

integral (I): The integral term is concerned with the accumulation of past errors. If the error has been present for an extended period, it will accumulate (integral of the error), and the controller will respond by changing the control output about a constant known as $K_i$, the integral gain constant.

Derivative (D): The derivative term is a prediction of future error, based on its rate of change. It provides a control output to counteract the rate of error change. The contribution of the derivative term to the overall control action is termed the derivative gain, $K_d$.

The PID control equation can be summed as:

$$[u(t) = K_p * e(t) + K_i * \int e(t)dt + K_d * \left(\frac{d}{dt}e(t)\right)] \quad (1)$$

Here, u(t) is the control signal, and e(t) is the error (difference between desired and actual state). The constants $K_p$, $K_i$, and $K_d$ are tuned to achieve optimal performance for each specific system.

## 2.2 Neuro-fuzzy regulator

A neuro-fuzzy regulator is an intricate control mechanism that fuses the principles of neural networks and fuzzy logic to govern intricate systems characterized by uncertainty or nonlinear behaviors. This regulator is structured into three fundamental components: fuzzification, fuzzy inference, and defuzzification. The fuzzification process employs membership functions to transform precise numerical inputs into fuzzy sets, while the fuzzy inference stage utilizes linguistic rules to ascertain the association between these inputs and the anticipated outputs. The defuzzification phase subsequently translates these fuzzy outcomes into a singular precise output value.

Within this system, the neural network element serves as a dynamic learning tool, refining control performance and acclimating variations within the system's behavior. By adjusting the variables of the fuzzy inference system with a set of input-output training data, it optimizes the system's responsiveness. The final control output is ascertained through the amalgamation of the outcomes of fuzzy inference and the parameters fine-tuned by the neural network.

A standard mathematical representation for the control output within this context may be formulated as CO(t) = f([X(t)], [θ]), where CO(t) denotes the control output at a given time t, $[X(t)]$ symbolizes the system's input vector, and $[\theta]$ signifies the specific parameters associated with the neuro-fuzzy regulator.

Employed across various domains such as industrial processing, robotics, autonomous technologies, and intelligent transport systems, neuro-fuzzy regulators provide adaptability to shifting conditions and encapsulate specialist understanding via fuzzy rule sets. By integrating the attributes of both neural networks and fuzzy logic, these regulators afford a level of control that is simultaneously precise and adaptable, catering to complex system demands.

## 2.3 Model Predictive Controller

The Model Predictive Controller (MPC) represents a sophisticated method of control that has been extensively employed across diverse industrial sectors. This control strategy leverages a dynamic model of a given system to forecast future responses and tailor control actions over a defined predictive period.

In the context of MPC, control challenges are characterized as optimization problems where the aim is to minimize a cost function. This function encapsulates vital aspects of system performance such as adherence to setpoints and efficiency of control, while simultaneously factoring in constraints. The quantifiable cost function constitutes a weighted aggregation of these elements.

Utilizing the dynamic model, MPC carries out simulations to foresee future system behavior, thereby enabling the optimization of control inputs. This involves considering a series of future time steps to evaluate the impacts of alternative control strategies, ensuring that optimal control inputs are determined while recognizing constraints and the intrinsic dynamics of the system.

MPC can manage constraints about both system outputs and control inputs, thus safeguarding the operation of the system within permissible boundaries. It utilizes computational techniques such as quadratic programming to expedite the resolution of the optimization challenge.

At each successive control interval, MPC administers solely the initial control action from the optimal sequence and readdresses the optimization problem with freshly updated data.

MPC's proficiency in managing constraints, integrating system dynamics, and real-time optimization of control strategies makes it an apt choice for intricate control applications. Its deployment spans areas such as chemical processing, energy systems, robotics, and self-governing vehicles. The methodology's efficacy in attaining targeted system performance, in conjunction with compliance with operational limits, underscores its value in contemporary control engineering.

# 3 Biomechanical Modeling

We commence the project by designing a robotic arm engineered for precise movements within a three-dimensional environment, particularly tailored for reaching tasks. This design process employs the Denavit-Hartenberg (D-H) parameters, a widely recognized method in robotics, to determine the robot's forward and inverse kinematic equations. An accompanying illustration offers a detailed anatomical view of the robot in its maximum extended position. This configuration is critical for our analysis, as it serves as the benchmark in our research for simulating the biomechanics underlying the controller's function. Based

on this schematic, we extrapolate and present a series of equations that define the robot's movement dynamics in the context of our study.

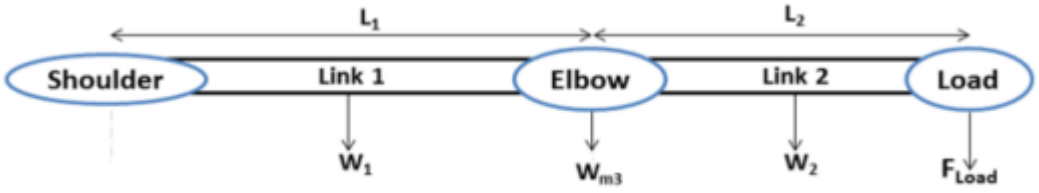


*Figure 4. Free Body diagram of robot*

*(Farman, M., Al-Shaibah, M., Aoraiath, Z., & Jarrar, F. (2018)*

We design our model based on the design of the three-degree-of-freedom robotic arm model described by Farman, M., Al-Shaibah, M., Aoraiath, Z., & Jarrar, F. (2018). Design of a three-degrees-of-freedom robotic arm. *International Journal of Computer Applications*, 179(37). It is defined by the equations below.

$$x = [\cos(\theta_{s_1}) * \left(L_s * \cos(\theta_{s_2}) + L_e * \cos(\theta_e + \theta_{s_2})\right)] \quad (2)$$

$$y = [\sin(\theta_{s_1}) * \left(L_s * \cos(\theta_{s_2}) + L_e * \cos(\theta_e + \theta_{s_2})\right)] \quad (3)$$

$$z = [\left(L_s * \sin(\theta_{s_2}) + L_e * \sin(\theta_e + \theta_{s_2})\right)] \quad (4)$$

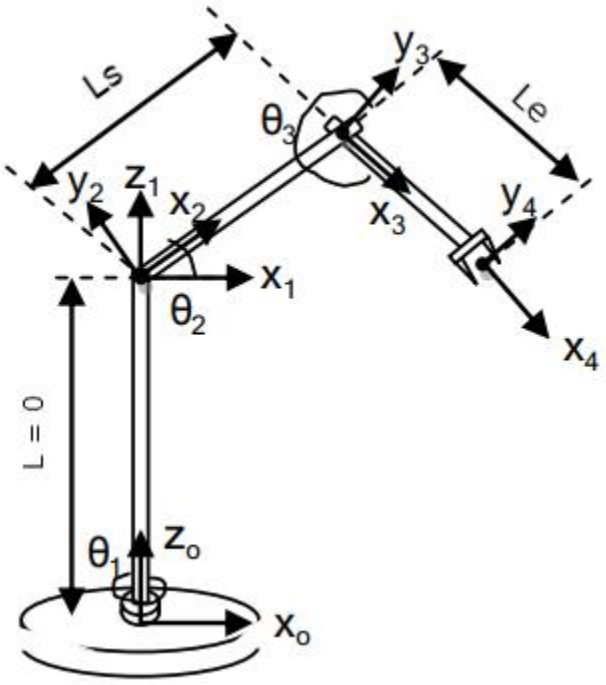


*Figure 5. Frame assignment for Kinematic Analysis*

*(Farman, M., Al-Shaibah, M., Aoraiath, Z., & Jarrar, F. (2018)*

The model includes the coordinates (x, y, z), $\theta_1$ and $\theta_2$ are angles for the shoulder for 2 degrees of freedom and theta3 is the elbow angle, $L_s$ is shoulder length and $L_e$ will be elbow length. For the construction of our model, we set values for $L_s$ and $L_e$ at 0.175 m, and the mass of the shoulder and elbow is 1 kg, aligning with the morphometry data derived from Macaca Mulatta monkeys (Cheng and Scott, 2000). The choice to utilize muscle morphometry data from monkeys, as opposed to humans, is guided by the comparable physiology, analogous mechanics, and evolution of movement, along with a rich array of studies investigating neural regions in motor planning and control. These studies tend to face fewer constraints in monkeys than in humans (Graham et al., 2003). Moreover, the physical dimensions of the monkey's limb closely correspond to our prior experiments with robotic arms, making it a pertinent comparison for future explorations.

Regarding the biomechanical system's responsiveness to muscle interaction, we can make estimations concerning muscle lengths. Given that the Virtual Muscle model (Cheng, Brown, and Loeb, 2000) encompasses intrinsic information about its nonlinear stretch-force and stretch-speed constituents, it permits the assumption that the velocity and length components of the 'spindle' activity are recognized by the system. We also infer that knowledge of stretch length and velocity enables the approximation of muscle lengths. Furthermore, simple geometric principles, such as the law of cosines, can be employed to ascertain muscle-tendon lengths for each muscle, based on motion dynamics.

*Table.1 Muscle Attachment Lengths used in the Model.*

| | | |
|---|---|---|
| Biceps | Elbow joint to the arm bone | 0.02919 m |
| | Elbow joint to the shoulder bone | 0.13581 m |
| Triceps | Elbow joint to the arm bone | 0.02148 m |
| | Elbow joint to the shoulder bone | 0.15864 m |
| Extensor | Shoulder joint to shoulder bone | 0.01481 m |
| | Shoulder joint to the back | 0.08127 m |
| Flexor | Shoulder joint to shoulder bone | 0.01481 m |
| | Shoulder joint to chest | 0.06121 m |
| Adductor | Shoulder joint to shoulder bone | 0.02158 m |
| | Shoulder joint to side bone | 0.09562 m |
| Abductor | Shoulder joint to shoulder bone | 0.02158 m |
| | Shoulder joint to the clavicle bone | 0.07125 m |

In the detailed biomechanical configuration, we meticulously designate anchoring points where muscles connect to the skeletal framework, thereby inducing a torque effect. These specific muscle attachment distances, clearly delineated in the accompanying table, are instrumental in our model. They not only determine the individual muscle lengths but also play a crucial role in deducing the torque resultant from forces exerted upon them.

Delving deeper, understanding the multifaceted interaction between muscles and the biomechanical apparatus allows for a more nuanced estimation of muscle lengths. The Virtual Muscle (VM) model, with its sophisticated design, encompasses comprehensive data about its non-linear dynamics, specifically the stretch-force and stretch-velocity relationships. Given this rich internal dataset, we can infer with confidence that the system possesses an intrinsic awareness of the "spindle" activity, covering both its velocity and length dimensions.

With the aforesaid stretch length and velocity parameters available, we can refine our approximations of muscle lengths. Moreover, to achieve a precise calculation of muscle-tendon lengths associated with each specific muscle relative to its range of movement, we leaned on fundamental geometric methodologies. Notably, the law of cosines emerged as an invaluable tool, providing a mathematically rigorous framework to decipher these lengths in correlation with the observed motion.

Lastly, the rotation restrictions for the 2 shoulder angles and elbow angles are delineated as [-0.872665, 2.61799], [-1.0472, 3.14159], and [0, 2.61799] rad, respectively.

# 4 Planning for a 3D Controller

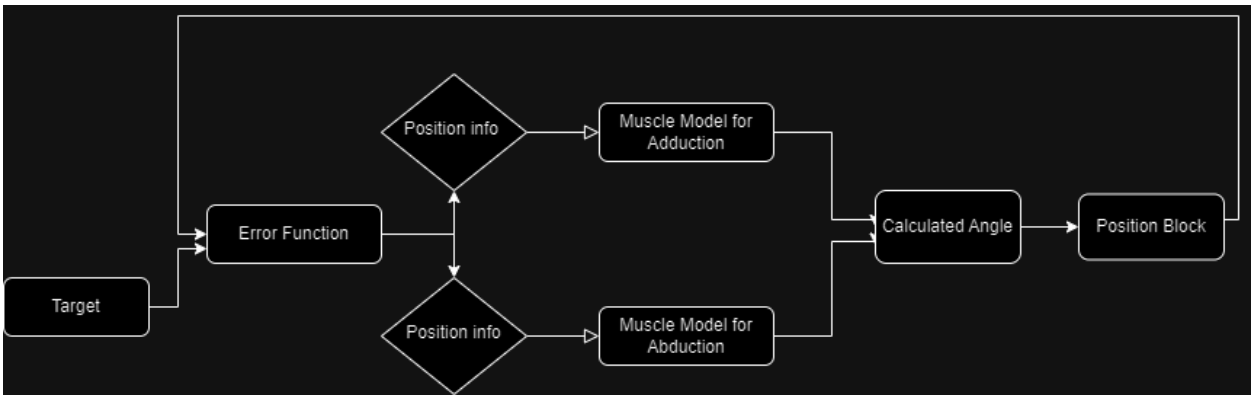


*Figure 6. Basic Planned Model of the controller used to Design the Simulink Model*

The illustrated figure delineates the methodical process of the model. It commences with the error function, which quantifies the difference between the desired target position and the model's instantaneous location. This discrepancy serves as an input to the position blocks. Here, a sophisticated algorithm decides on the specific muscle that needs activation, as well as quantifies the degree of its movement, taking into account the internal dynamics of the model.

After this, the muscle models come into play. Using biomechanical principles, they estimate the muscle force output essential for the arm's mobilization. It's pivotal to note that different muscles can produce varying force outputs depending on their physiological attributes and the model's current state.

Once the force output is determined, it is paired with the identified active muscle. This combination is then utilized to compute the arm's terminal angular position. This angular data assists the position block in calculating the arm's exact location in a three-dimensional space.

This newly computed position feeds back into the error function, creating a feedback loop. This continuous loop ensures that the model adjusts its movement iteratively, refining its position with each cycle, aiming

for precision until the arm aligns with the target position. The iterative nature of this process ensures accuracy and efficiency in the model's movement trajectory.

## 4.1 Virtual Muscles

The Virtual Muscles for the 3D arm were constructed utilizing muscle morphometry data from Macaca Mulatta monkeys, as found in prior research (Cheng and Scott, 2000). A comprehensive review of the formation and application of the Virtual Muscle models is not included here, as it is thoroughly documented in the existing literature. To integrate these muscles into the previously detailed biomechanical model, each muscle was situated on the virtual arm, with careful consideration to prevent overstretching or under-stretching, in alignment with the design constraints of the Virtual Muscle and the boundaries of joint rotation. The software associated with this model necessitates two specific inputs to enable a realistic simulation of muscle behavior: (a) muscle activation or recruitment, normalized within a range of 0 to 1, and (b) the combined length of muscle and tendon. Supplying valid input values to the Virtual Muscle model yields a force output, which can then be employed to solve equations (7.1) - (7.6). Comprehensive information regarding the Virtual Muscle software, its design, or its utilization is available in the work of Cheng, Brown, and Loeb (2000).

# 5 Creating the Controller

The adaptive spinal-like controller utilized in this research, building upon methodologies delineated in Chapter 6 and earlier robotic studies, has been tailored and expanded to focus on 3D joint movement. The model's enhancement involves the introduction of an additional antagonist muscle pair, namely the Adductor/Abductor, at the shoulder joint, which adds complexity to the system. The hand-target error, a critical aspect of the control algorithm, is computed by measuring the coordinate difference between the hand's current position and the target's location in a 3D space. The distributed error data is then

meticulously processed by the motoneurons in both the shoulders and elbows, enabling the calculation of the co-activation values essential for the virtual muscle models.

Co-activation within the interneurons is quantified on a scale ranging from 0 to 1, where a value of 1 represents full co-activation, signifying an equal amount of activation to both muscles in the pair, and 0 indicates no co-activation. The summation of the normalized inputs from these components to the interneurons is skillfully utilized to dictate muscle recruitment. This process translates into an activation level input for each involved muscle group, constrained within the [0, 1] range to align with the specifications of the Virtual Muscle model.

Once activated, the Virtual Muscle produces a force output in Newtons, which plays a pivotal role in solving the biomechanical equations. Concurrently, this activation triggers changes in geometry, leading to alterations in muscle-tendon length across individual muscle groups. The resolution of these equations yields critical data concerning joint angles, velocities, and other associated kinematic variables.

Subsequently, with the derived information, the ‘new’ hand position can be geometrically pinpointed with precision, effectively serving as a substitute for vision-based tracking. This methodological approach presents a robust framework for understanding complex muscle interactions and 3D spatial movement, holding significant implications for the development of advanced biomechanical and robotic systems.

# 6 Experimental Procedures

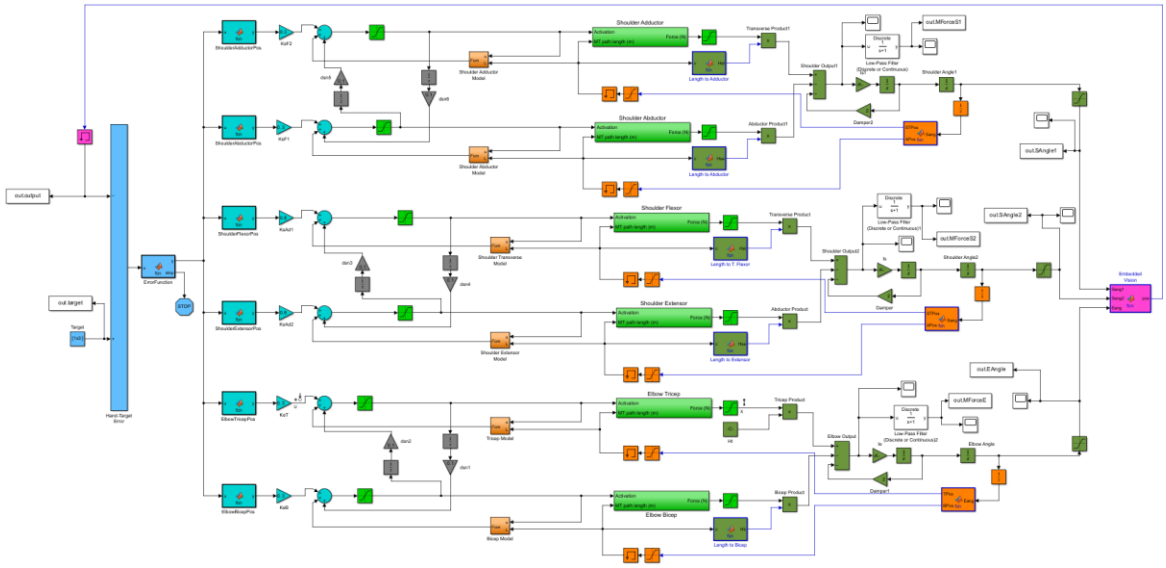

*Figure 7.MATLAB Simulink Model for 3D Corticospinal Controller*

To expand on the process, we commence by incorporating an additional muscle model into the pre-existing 2D model. Specifically, an antagonistic muscle pair, comprised of the Adductor and Abductor, is integrated into the model. The first step in this integration involves adding position blocks. These blocks are designed to intake data from the z-axis, which is obtained from the error function associated with the model. This data is then processed to determine the level and specificity of muscle activation.

To normalize the inherent non-linearities within the virtual muscle models, a sigmoid normalization function, (as recommended by Stefanovic, F., & Galiana, H. L. (2014). An adaptive spinal-like controller: tunable biomimetic behavior for a robotic limb. *BioMedical Engineering OnLine*, 13, 151.), is applied within the position block. Following this normalization, the output is fed into the virtual muscle models. These models, in turn, generate a force output corresponding to the involved muscles.

Subsequently, this force output is multiplied by the muscle length. The muscle length is computed based on feedback data. The result of this multiplication provides the torque that the muscle requires to adjust its motion to reach the specified z-coordinate.

Next, the resultant outputs from the antagonistic muscle pair are summed. The resulting total provides a final output angle. This angle guides the movement of the 3D arm model, allowing it to reach the final target location.

The process is not complete, however. The output angle, combined with the angles at the elbow and other shoulder angle for the x and y coordinates, are inputted into the vision block. Here, the final position of the model is calculated. This calculation is based on the coordinate equations that were detailed in earlier sections.

The resulting position data is then fed back into the error function. This allows for the calculation of a new error, which in turn, provides a basis for the subsequent operation of the model. This iterative process continues, driving the model's continued evolution and adjustment.

In our research, we meticulously structured experimental protocols to illustrate basic reaching maneuvers within a three-dimensional plane positioned inside a predefined accessible workspace. This experimental arrangement serves two primary objectives:

- Firstly, to offer a detailed insight into the functionality and adaptability of the controller when navigating the 3D space.
- and secondly, to ascertain its performance relative to distinct target destinations.

For the trajectory planning phase, we have chosen an array of diverse points within the 3D environment. Every trajectory starts from a consistent origin point, denoted as (0, 0, 0), and progresses towards the predetermined arbitrary point. This systematic approach ensures comprehensive coverage of the

workspace and provides a rigorous assessment of the controller's efficiency and precision in path planning and execution.

# 7 Results

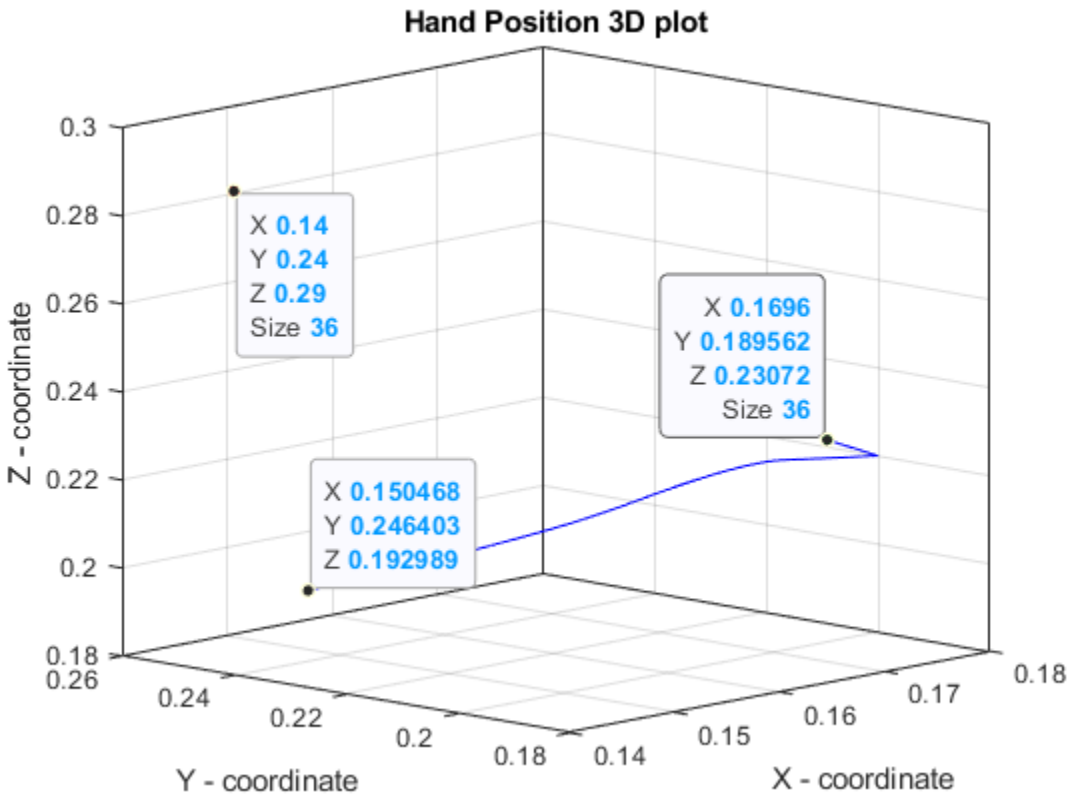


*Fig.8 3D Plot of Hand Position in Space*

The figure in discussion provides a detailed trajectory of the model's movement from its starting position to its destination. Commencing at an initial coordinate (0.1696, 0.189562, 0.23072), the model's movement is guided by data derived from the error function block.

For the z-coordinate, a notable trend emerges at an initial peak at 0.22, which subsequently drops to a level of 0.19. The x-coordinate, on the other hand, demonstrates an interesting behavior. After an initial rise to 0.17, it begins its descent toward its target value of 0.14. Interestingly, it stabilizes slightly above

the target, settling at 0.15. This stabilization is noteworthy, as it suggests that the model's movement closely approximates the intended target with minimal deviation.

The y-coordinate presents another dynamic. Coinciding with the peak of the x-coordinate at 0.17, the y-coordinate increases to 0.20. It doesn't stop there but continues its ascent until it meets its preset target of 0.24.

Once all these movements across the three coordinates converge, the simulation terminates. The final resting position of the model arm, as captured at this concluding moment, is (0.15, 0.24, 0.19). This intricate movement trajectory underscores the model's intricate navigation capabilities, showing how it maneuvers within a three-dimensional space to approach its target location.

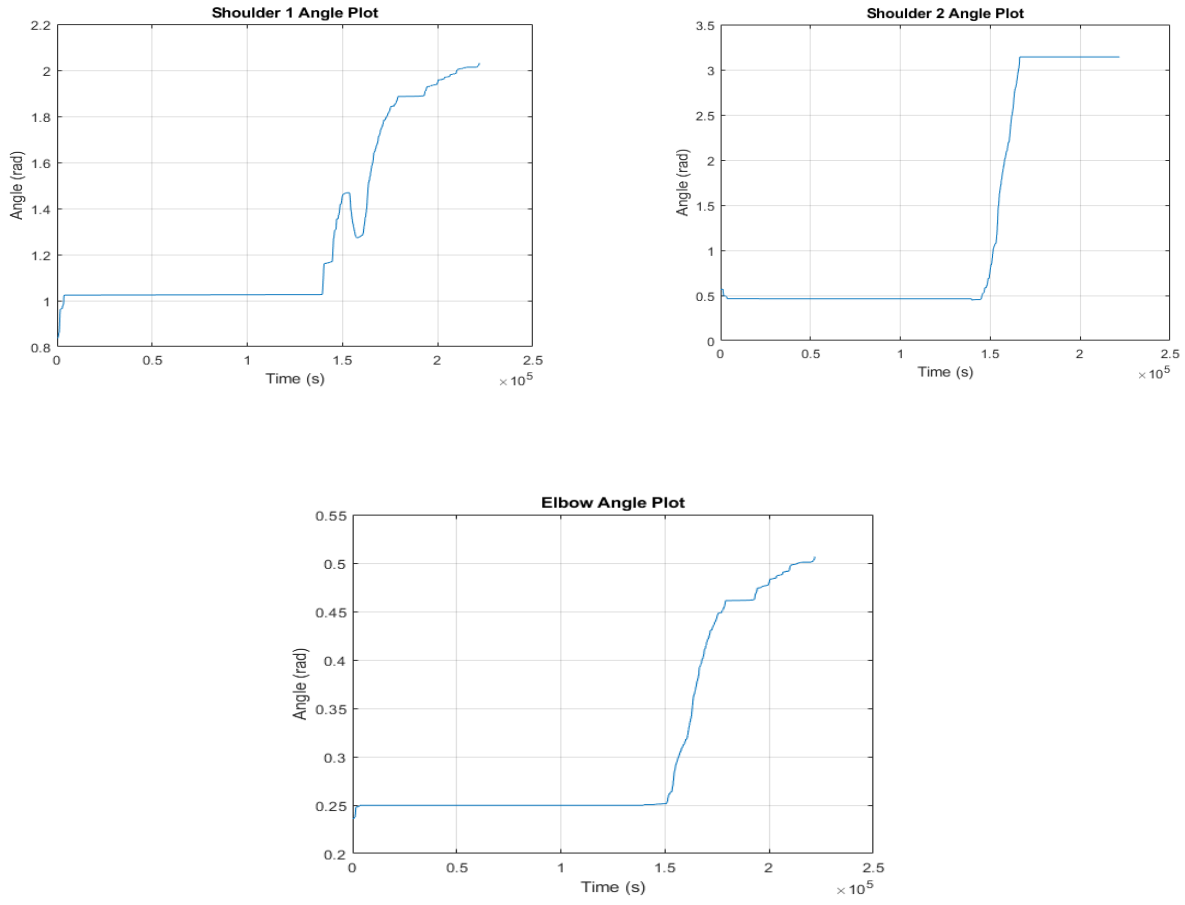


*Figure 9.Angle plot of all 3-Muscle pair with respect to time*

The presented angle plots offer a comprehensive visualization of the temporal dynamics in the shoulder and elbow angles as the model moves closer to its predefined target. As time progresses, there is a pronounced increase in both the Elbow and Shoulder Angle 2. These angles play a crucial role in manipulating the x and y coordinates of the model. In contrast, Shoulder Angle 1, which primarily influences the z-coordinate, experiences a nuanced decline from 1.5 rad, bottoming out at 1.3 rad, before ascending again to attain a value of 2 rad.

It's of significant importance to underscore that these angular shifts are grounded in the parameters set by human anatomical restrictions. The elbow angle's permissible range is defined between 0 rad and 2.61799 rad. In parallel, the two shoulder angles have been delineated with specific constraints: the first shoulder angle oscillates between -0.872665 rad and 2.61799 rad, while the second shoulder angle is demarcated within the range of -1.0472 rad up to 3.14159 rad. These anatomical boundaries ensure the model's movement mimics realistic human motion, preserving both the integrity and authenticity of the simulation.

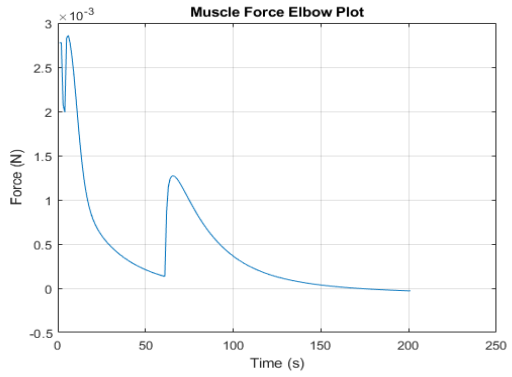


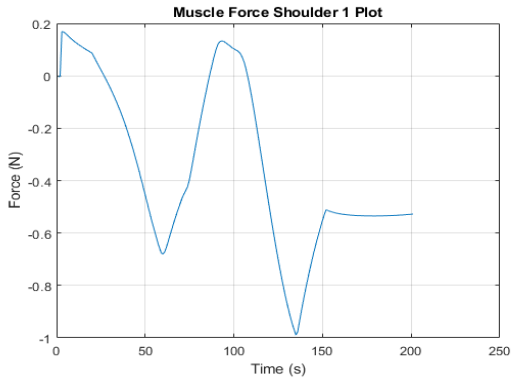

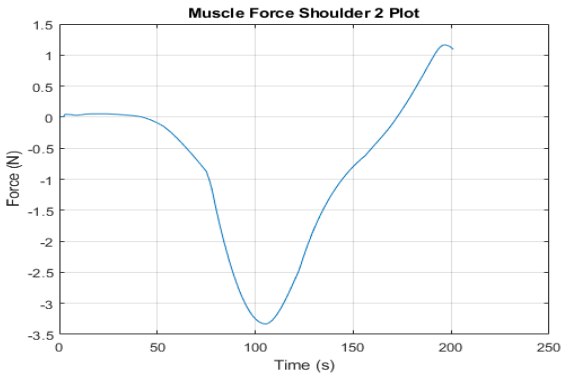


*Figure 10.Muscle Force Plot of all 3-Muscle pair with respect to time*

In the provided visual data, the muscle forces for distinct joints are portrayed, having undergone refinement via a low-pass filter to enhance the interpretability of the data. Upon inspection of the elbow's muscle force trajectory, one can discern that it reaches a zenith at 0.03N. This specific trajectory is indicative of the muscle's compensatory actions, driven by the input from the error function. This compensation is in direct response to the positional modifications exhibited by the model during its operation.

In a parallel observation, the force plot for Shoulder 1 depicts a dynamic adjustment pattern tailored to the model's requirements. The highest force exerted by this muscle is roughly 0.2 N. This nuanced modulation ensures the system remains responsive to real-time changes, optimizing movement.

On the other hand, the muscle force plot for Shoulder 2 is particularly intriguing. Initially, there's a pronounced decrease in force, which can be associated with preparatory or initial positioning. This decline is promptly succeeded by a surge, with the force eventually plateauing at 1.3 N. Such a pattern suggests a powerful engagement of the muscle, ensuring that the endpoint or target is not only reached but also stabilized efficiently.

# 8 Discussion

In this research, we unveil the advancements of the CSC model specifically tailored for 3D target-reaching tasks in assistive robotics, highlighting its profound potential for extended investigative applications. Drawing inspiration from the foundational work on a 2D Adaptive Spinal-like Controller introduced by Stefanovic, F., & Galiana, H. L. (2014). An adaptive spinal-like controller: tunable biomimetic behavior for a robotic limb. *BioMedical Engineering OnLine*, 13, 151, our methodology has been to adapt and evolve this foundational model to meet the complexities of a 3D environment, and then rigorously test it through structured experiments.

A distinguishing feature of our work is its pioneering nature; as of our current understanding, there isn't any feedback controller explicitly architected for nuanced 3D control. This research's primary objective is not just to posit the possibility of a 3D controller, but also to underscore its immediate applicability for elementary reaching activities, even in its nascent stages.

An intriguing aspect of our model is its capacity to emulate intricate interconnections between various muscle models, thus enhancing its complexity. Such a design not only renders the model more representative of human anatomy but also paves the way for its application in advanced academic research and as a cost-efficient substitute in prosthetic innovations.

By fine-tuning and optimizing the model's parameters, we can engineer its trajectory to achieve specific orientations within desired timeframes. This inherent flexibility, marked by its capability to distinctively handle hand kinematics and dynamics, designates the model as highly adaptable for practical applications, extending to studies focused on primate reaching behavior. Our vision for the next phase of research is ambitious. We aim to integrate a comprehensive wrist model, in harmony with the arm architecture, to holistically represent the arm's layered intricacies. Such an enhancement could drastically elevate the model's capacity to execute tasks of increased complexity.

In this detailed investigation, we delved into the intricacies of hand trajectory modulation and its path in the context of 3D space, emphasizing the pivotal role played by adjusting the ratios of error projection weights corresponding to each muscle model. This technique of gain manipulation isn't novel per se; it was adeptly demonstrated in trajectory shaping for center outreaching tasks by Stefanovic, F., & Galiana, H. L. (2014). An adaptive spinal-like controller: tunable biomimetic behavior for a robotic limb. *BioMedical Engineering OnLine*, 13, 151. Our experimental model applies a similar methodology, offering an adept mechanism to fine-tune hand motion dynamics and meticulously design pathways in 3D space.

Notably, this mode of trajectory adjustment offers a nuanced alternative to the conventional methods of motion kinematics planning, as elaborated by Flash and Hogan in 1985. Through manipulation of the gain ratios linked to pertinent components, one possesses the capability to modify the trajectory curvature and symmetry of the hand's movement, offering flexibility in shaping its course in a multitude of ways.

Post meticulous calibration, our data robustly indicate that a significant proportion of the crafted 3D motion trajectories mirror the patterns and nuances inherent to biological movements in nature. These gain ratios, which we meticulously explored, could be analogously perceived in a biological context. They might represent shifts in the recruitment of specific cellular pathways or variances in synaptic interactions bridging error projections with spinal pre-motor circuits. This perspective aligns with and extends discussions from seminal works, notably those by Grantyn and Berthoz in 1985 and later by Gandhi and Katnani in 2011.

# 9 Conclusion

The Adaptive Spinal-like Controller (ASC), as referenced in earlier scholarly endeavors, stands as a meticulously crafted computational representation of the spinal cord. Its principal design is geared

towards achieving fluid and coordinated activities in an apparatus configured with multiple joints and muscles. Characterized by its versatility, the ASC serves as an epitome of sensory-driven limb management, endorsing a slew of capabilities: it fosters adaptive control, exhibits rapid responsiveness to stimuli, enables nuanced movement adjustments, and showcases proficiency in both time-based and space-oriented scaling. Furthermore, it excels in pinpoint target tracking facilitated by motor plants and optimally adjusted error projection weights.

In this comprehensive study, we pioneered the unveiling of the CSC model, a sophisticated design tailored for orchestrating 3D motion patterns and trajectory schematics—a dimension not traversed in preceding controller-centric research. Our empirical demonstrations elucidate its dexterity in orchestrating multi-joint robotic arm navigations toward designated objectives.

Our collated data strongly indicate the controller's adaptability to 3D robotic frameworks, seamlessly aligning with biological motion paradigms cataloged in academic literature. This study's modern-day implications are profound, given the controller's intrinsic tunability, earmarking it as an invaluable precursor for prosthetic system evolution. Its broader applications stretch into future endeavors where researchers can employ this controller as a foundational tool to delve into broader terrains of robotic mechanics and human prosthetic innovations. Such prospects encompass the integration of a larger set of muscle pairs to cater to nuanced movements, the assimilation of advanced non-linear muscle architectures, the refinement of inter-joint torque dynamics, and the adoption of cutting-edge muscle simulations. The latter would ideally supersede the extant virtual iterations that draw inspiration from primate physiology. An even more ambitious trajectory, stemming from this investigative base, would be the conception and development of prosthetics modeled on intricate human anatomical specifications, sidestepping the primate-centric blueprints that anchored this present study.

# 10 References

1. Palastanga, N., Field, D., & Soames, R. (2006). Anatomy and human movement: structure and function.
2. Mow, V. C., Kuei, S. C., Lai, W. M., & Armstrong, C. G. (1992). Biphasic creep and stress relaxation of articular cartilage in compression? Theory and experiments. Journal of biomechanical engineering.
3. Hasler E, Herzog W, Wu J, Müller W, Wyss U. (1999). Articular cartilage biomechanics: theoretical models, material properties, and biosynthetic response. Crit Rev Biomed Eng, 27:415-88.
4. Debicki D, Gribble P. (2004). Inter-Joint Coupling Strategy During Adaptation to Novel Viscous Loads in Human Arm Movement. J Neurophysiol, 92:754-765.
5. Benjamin, M., Ralphs, J. R. (2008). Fibrocartilage in tendons and ligaments — an adaptation to compressive load. Journal of Anatomy.
6. Hayes, W. C., & Mockros, L. F. (1971). Viscoelastic properties of human articular cartilage. Journal of applied physiology.
7. Kearney, R. E., & Stein, R. B. (1997). Parameter estimation techniques for neuromuscular control systems. IEEE reviews in biomedical engineering.
8. Bagesteiro, L. B., & Sainburg, R. L. (2002). Handedness: dominant arm advantages in control of limb dynamics. Journal of Neurophysiology.
9. Ludvig, D., & Kearney, R. E. (2007). Estimation of viscoelastic joint parameters from torque-angle data. IEEE Transactions on Biomedical Engineering.
10. Widmaier, E. P., Raff, H., & Strang, K. T. (2011). Vander's human physiology.
11. Huxley, A.F. (1957). Muscle structure and theories of contraction. Progress in Biophysics and Biophysical Chemistry, 7, 255-318.

12. Lloyd, D.G., & Buchanan, T.S. (1996). A model of load sharing between muscles and soft tissues at the human knee during static tasks. Journal of Biomechanical Engineering, 118(3), 367-376.
13. Roberts, T.J., & Azizi, E. (2011). Flexible mechanisms: the diverse roles of biological springs in vertebrate movement. The Journal of Experimental Biology, 214(3), 353-361.
14. Cheng, E.J., & Loeb, G.E. (2008). Force feedback from mammalian muscle spindles during physiological conditions. In Neuroinformatics for Neuromodulation (pp. 141-164). Springer, New York, NY.
15. Song, D., Lan, N., Loeb, G.E., & Gordon, J. (2008). Model-based sensorimotor integration for multi-joint control: development of a virtual arm model. Annals of Biomedical Engineering, 36(6), 1033-1048.
16. Hill, A.V. (1938). *The heat of shortening and the dynamic constants of muscle*. Proceedings of the Royal Society of London.
17. Zajac, F.E. (1989). *Muscle and tendon: properties, models, scaling, and application*. Critical Reviews in Biomedical Engineering.
18. Song, D., et al. (2008). *Model-based sensorimotor integration for multi-joint control*. Annals of Biomedical Engineering.
19. Cheng, E.J., & Loeb, G.E. (2008). *Neuroinformatics for Neuromodulation*. Springer.
20. Roberts, T.J., & Azizi, E. (2011). *Roles of biological springs in movement*. The Journal of Experimental Biology.
21. Lloyd, D.G., & Buchanan, T.S. (1996). *Load sharing between muscles and soft tissues*. Journal of Biomechanical Engineering.
22. Farman, M., Al-Shaibah, M., Aoraiath, Z., & Jarrar, F. (2018). Design of a three-degrees-of-freedom robotic arm. *International Journal of Computer Applications*, 179(37).

23. Stefanovic, F., & Galiana, H. L. (2014). An adaptive spinal-like controller: tunable biomimetic behavior for a robotic limb. *BioMedical Engineering OnLine*, 13, 151.
24. Cheng, E. J., Brown, I. E., & Loeb, G. E. (2000). Virtual muscle: a computational approach to understanding the effects of muscle properties on motor control. Journal of Neuroscience Methods, 101, 117–130.
25. Stefanovic, F. (2013). Multi-muscle arm movements without planning: Proposing a tunable, scalable and robust biomimetic controller. (Doctoral dissertation, McGill University). Department of Biomedical Engineering, Montreal, Quebec, Canada.
26. Stefanovic, F., & Galiana, H. L. (2014). An adaptive spinal-like controller: tunable biomimetic behavior for a robotic limb. BioMedical Engineering OnLine, 13(151)
27. Stefanovic, F., & Galiana, H. L. (2014). A Simplified Spinal-Like Controller Facilitates Muscle Synergies and Robust Reaching Motions. IEEE Transactions on Neural Systems and Rehabilitation Engineering, 22(1), 77.
28. Stefanovic, F., & Galiana, H. L. (2016). Efferent Feedback in a Spinal-Like Controller: Reaching with Perturbations. IEEE Transactions on Neural Systems and Rehabilitation Engineering, 24(1).
29. Cheng, E. J., & Scott, S. H. (2000). Morphometry of Macaca mulatta Forelimb. I. Shoulder and Elbow Muscles and Segment Inertial Parameters. Journal of Morphology, 245, 206–224.

# 11 Appendix A

Here we present some more of the simulation results in graphs for better understanding and learning.

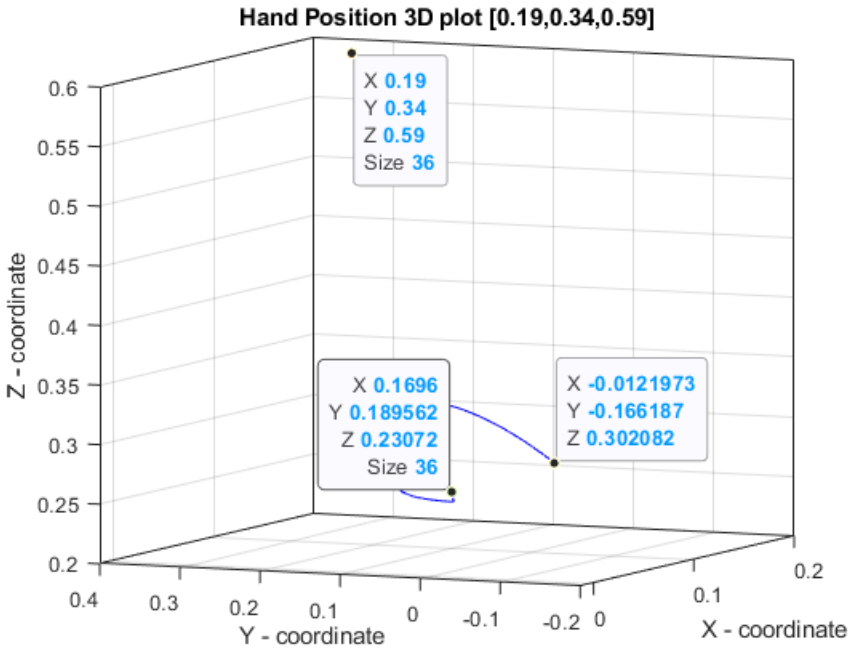


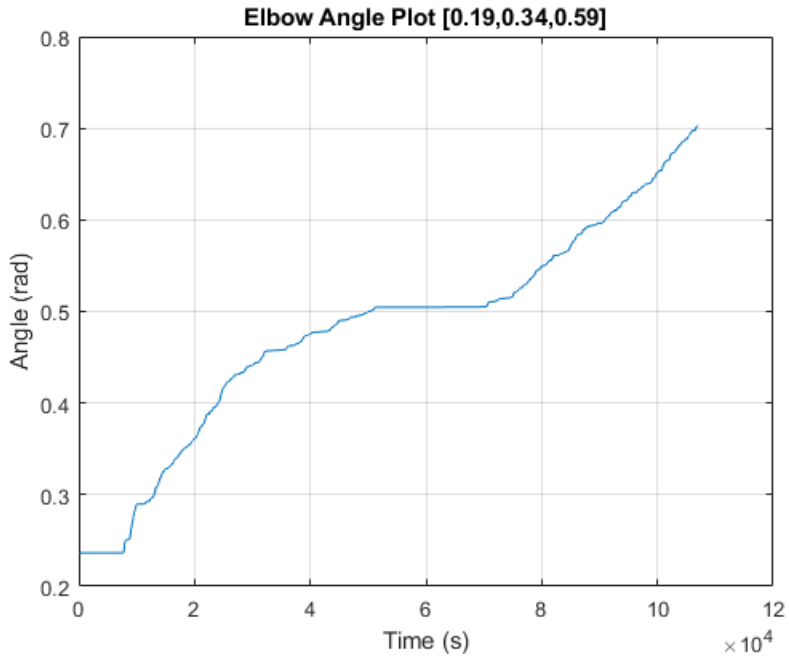

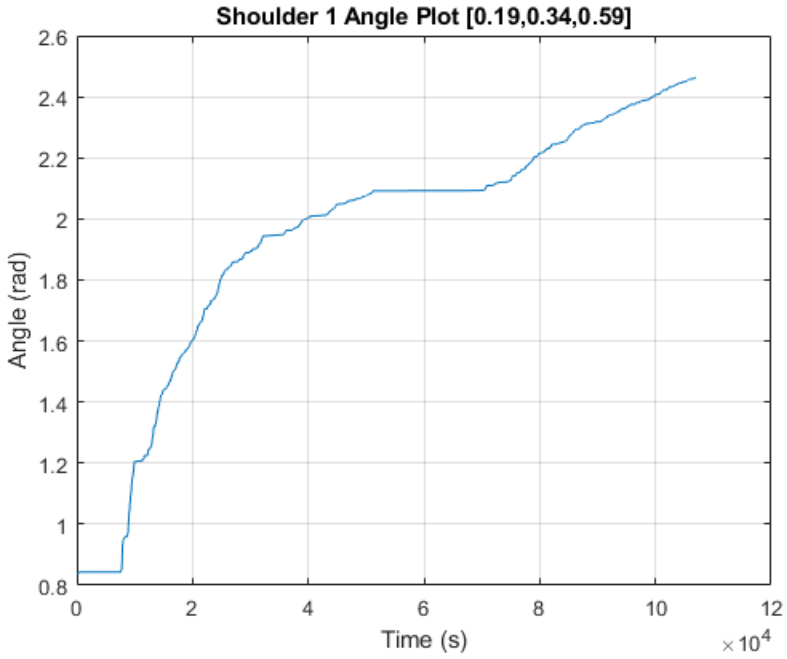
Shoulder 1 Angle Plot [0.19,0.34,0.59]
Angle (rad)
Time (s)
×10^4
2.6
2.4
2.2
2
1.8
1.6
1.4
1.2
1
0.8
0
2
4
6
8
10
12

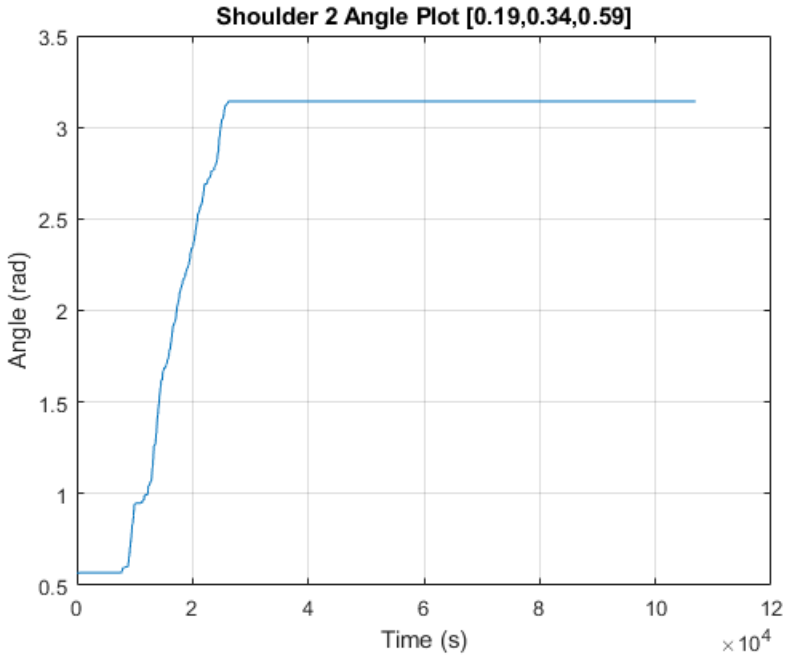
Shoulder 2 Angle Plot [0.19,0.34,0.59]
Angle (rad)
Time (s)
×10^4
3.5
3
2.5
2
1.5
1
0.5
0
2
4
6
8
10
12

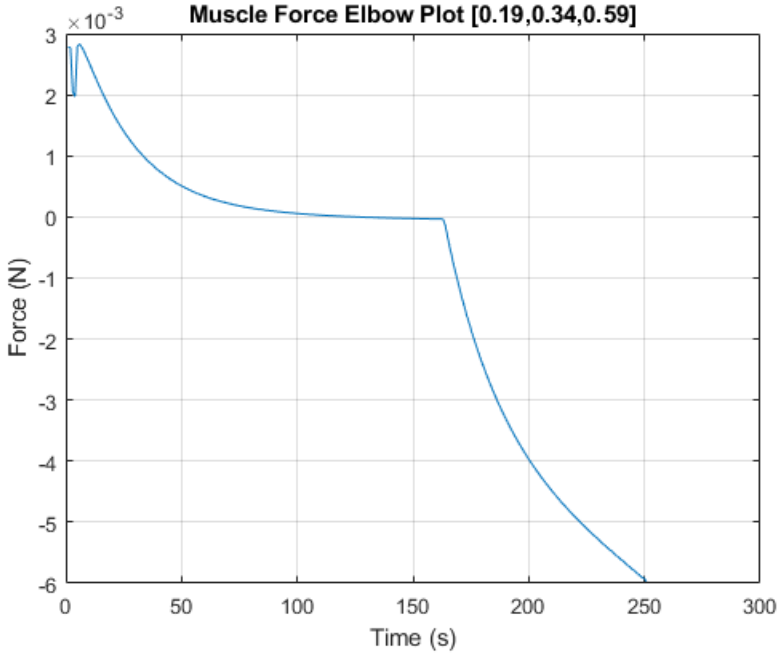
Muscle Force Elbow Plot [0.19,0.34,0.59]
×10^-3
3
2
1
0
-1
-2
-3
-4
-5
-6
Force (N)
0
50
100
150
200
250
300
Time (s)

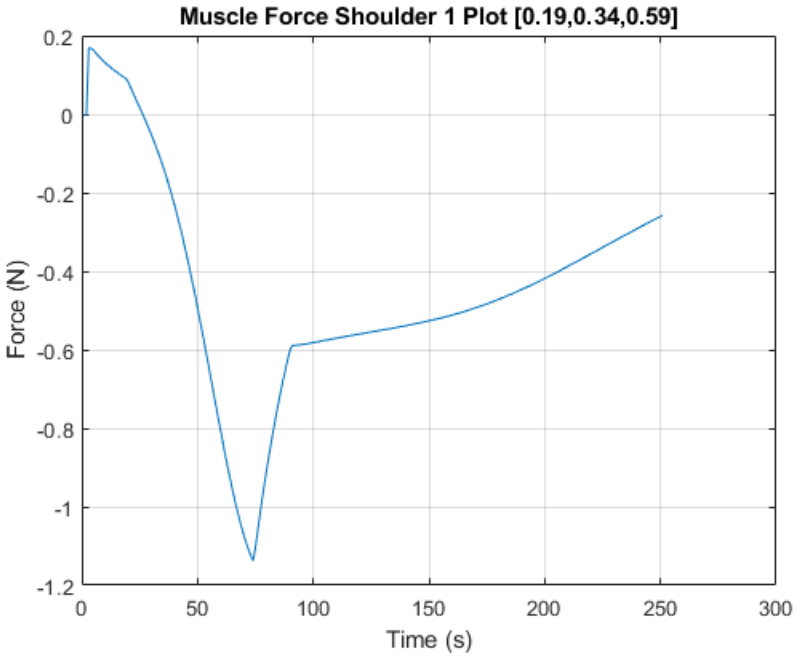
Muscle Force Shoulder 1 Plot [0.19,0.34,0.59]
0.2
0
-0.2
-0.4
-0.6
-0.8
-1
-1.2
Force (N)
0
50
100
150
200
250
300
Time (s)

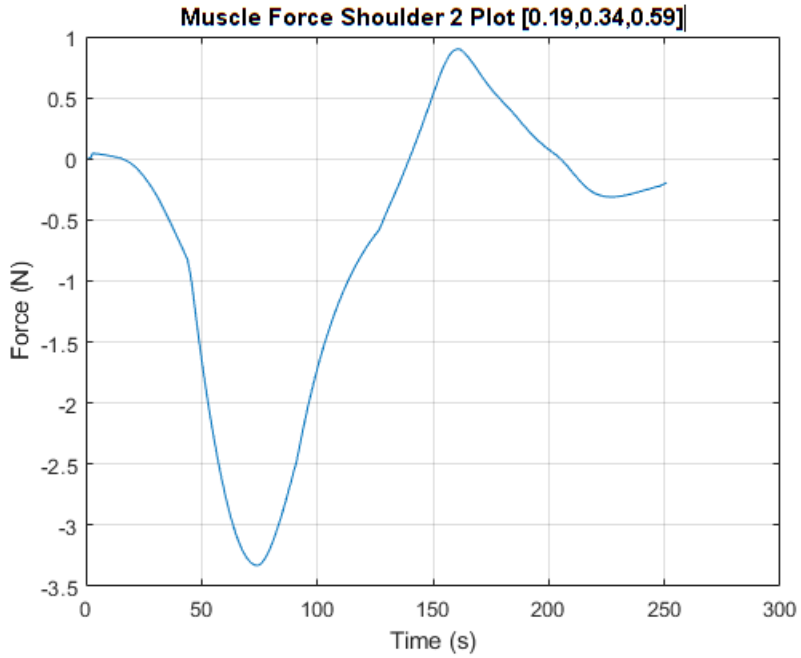
Muscle Force Shoulder 2 Plot [0.19,0.34,0.59]
Force (N)
Time (s)
1
0.5
0
-0.5
-1
-1.5
-2
-2.5
-3
-3.5
0
50
100
150
200
250
300

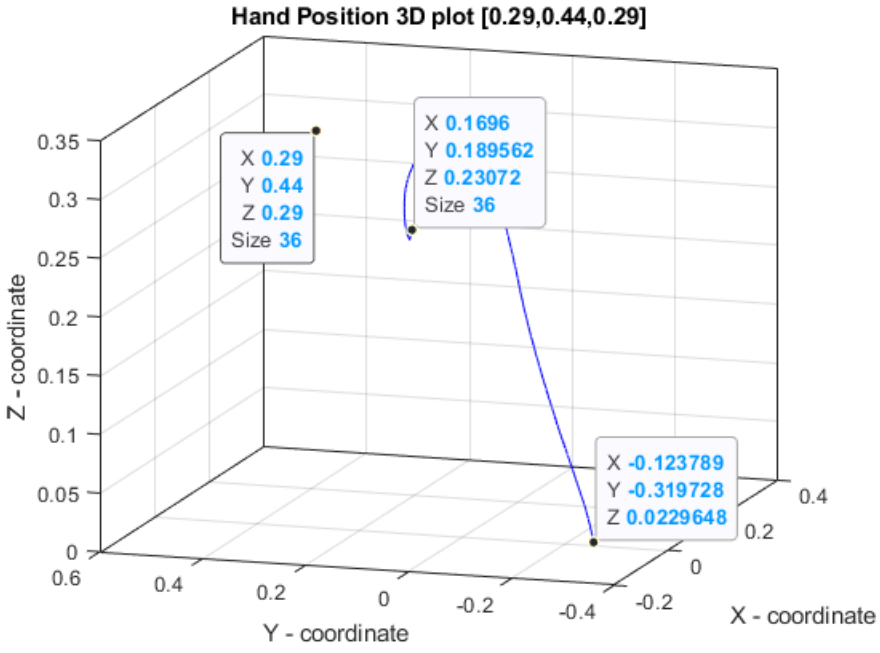
Hand Position 3D plot [0.29,0.44,0.29]
X 0.29
Y 0.44
Z 0.29
Size 36
X 0.1696
Y 0.189562
Z 0.23072
Size 36
X -0.123789
Y -0.319728
Z 0.0229648
Z - coordinate
Y - coordinate
X - coordinate
0.35
0.3
0.25
0.2
0.15
0.1
0.05
0
0.6
0.4
0.2
0
-0.2
-0.4
0.4
0.2
0
-0.2

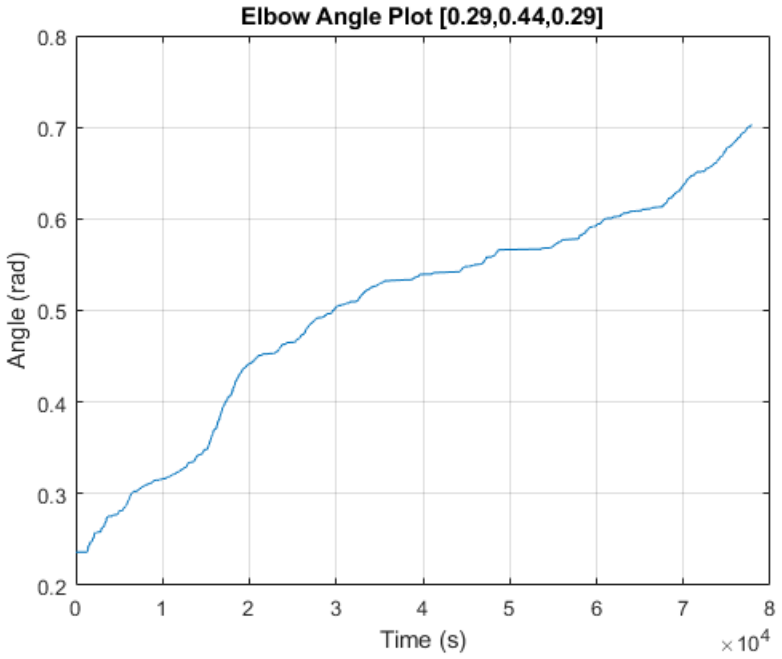
Elbow Angle Plot [0.29,0.44,0.29]
Angle (rad)
Time (s)
0.8
0.7
0.6
0.5
0.4
0.3
0.2
0
1
2
3
4
5
6
7
8
×10^4

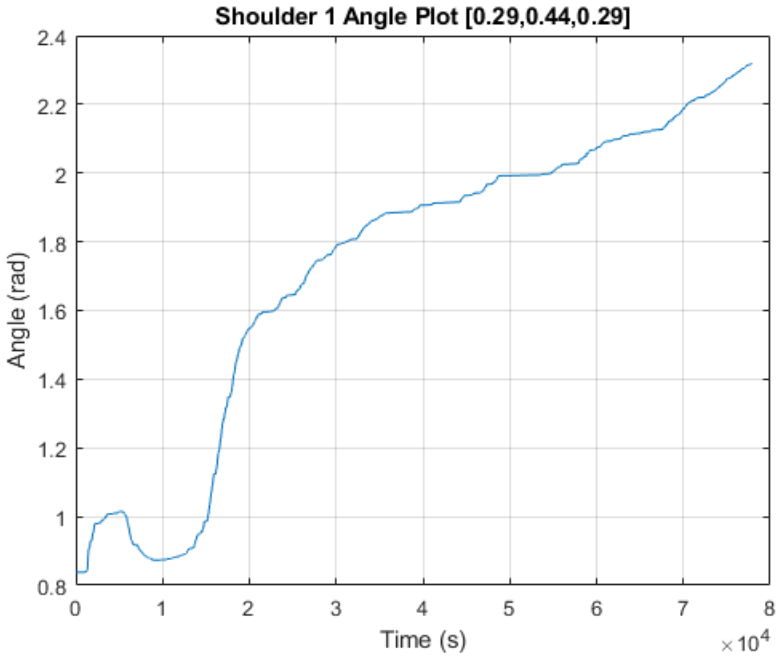
Shoulder 1 Angle Plot [0.29,0.44,0.29]
Angle (rad)
Time (s)
2.4
2.2
2
1.8
1.6
1.4
1.2
1
0.8
0
1
2
3
4
5
6
7
8
×10^4

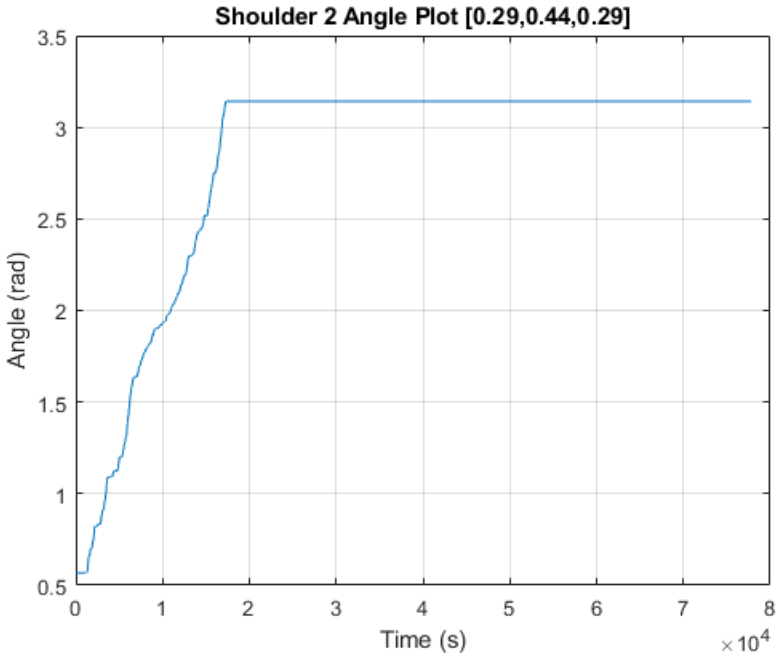
Shoulder 2 Angle Plot [0.29,0.44,0.29]
Angle (rad)
Time (s)
×10^4
3.5
3
2.5
2
1.5
1
0.5
0
1
2
3
4
5
6
7
8

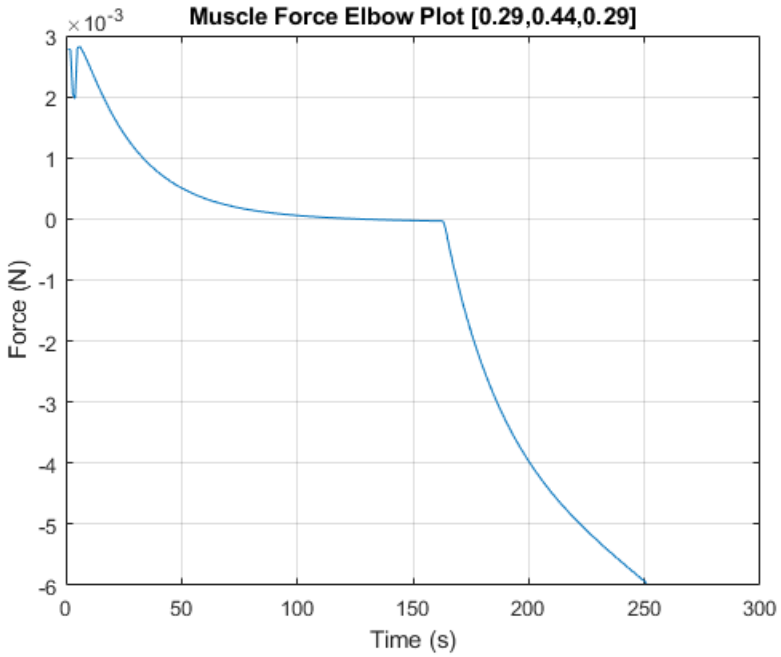
Muscle Force Elbow Plot [0.29,0.44,0.29]
×10^-3
Force (N)
Time (s)
3
2
1
0
-1
-2
-3
-4
-5
-6
0
50
100
150
200
250
300


Muscle Force Shoulder 1 Plot [0.29,0.44,0.29]
Force (N)
Time (s)
0.4
0.2
0
-0.2
-0.4
-0.6
-0.8
-1
-1.2
0
50
100
150
200
250
300

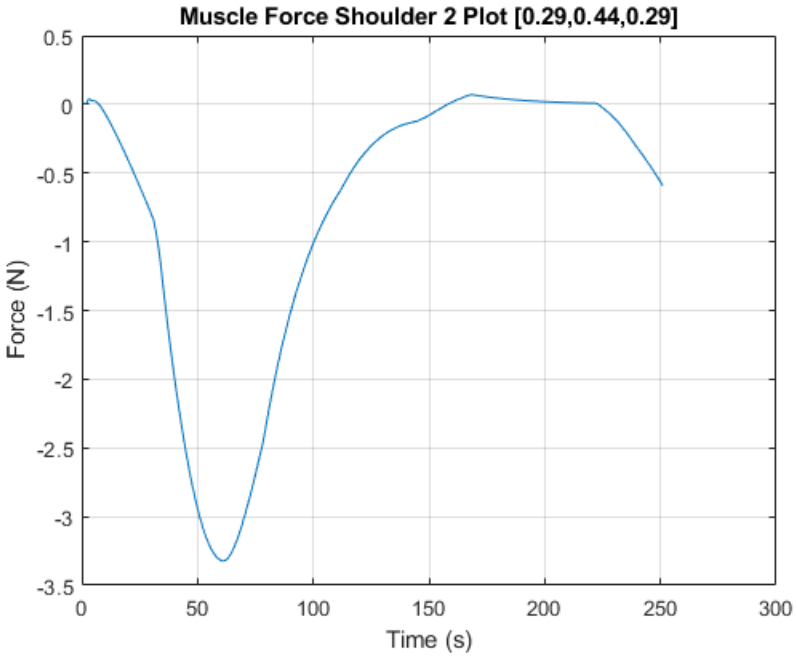
Muscle Force Shoulder 2 Plot [0.29,0.44,0.29]
Force (N)
Time (s)
0.5
0
-0.5
-1
-1.5
-2
-2.5
-3
-3.5
0
50
100
150
200
250
300

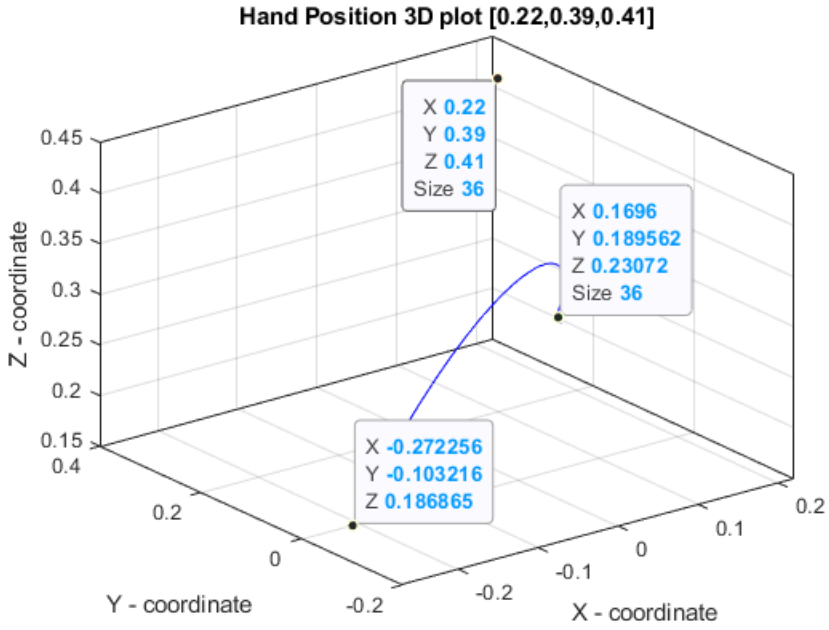
Hand Position 3D plot [0.22,0.39,0.41]
X 0.22
Y 0.39
Z 0.41
Size 36
X 0.1696
Y 0.189562
Z 0.23072
Size 36
X -0.272256
Y -0.103216
Z 0.186865
Z - coordinate
Y - coordinate
X - coordinate

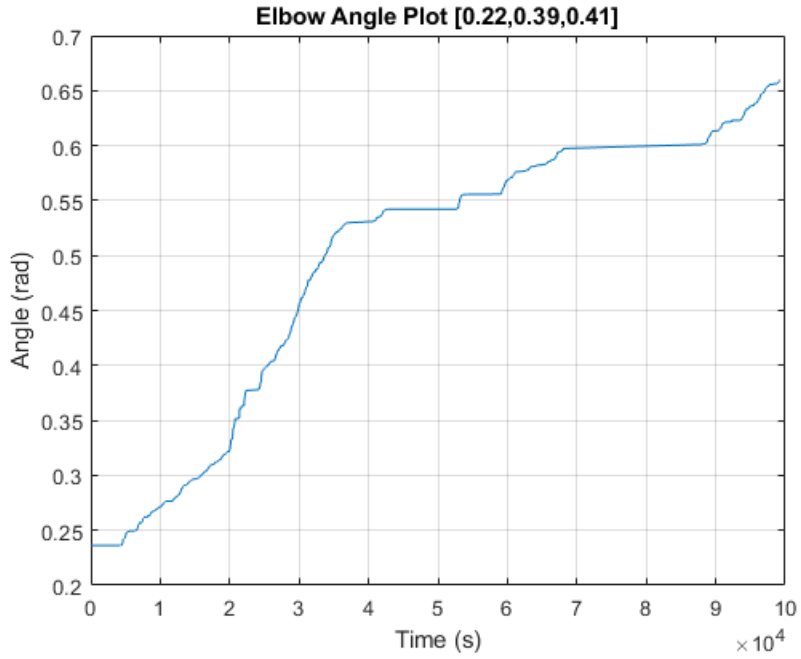
Elbow Angle Plot [0.22,0.39,0.41]
Angle (rad)
Time (s)
×10^4

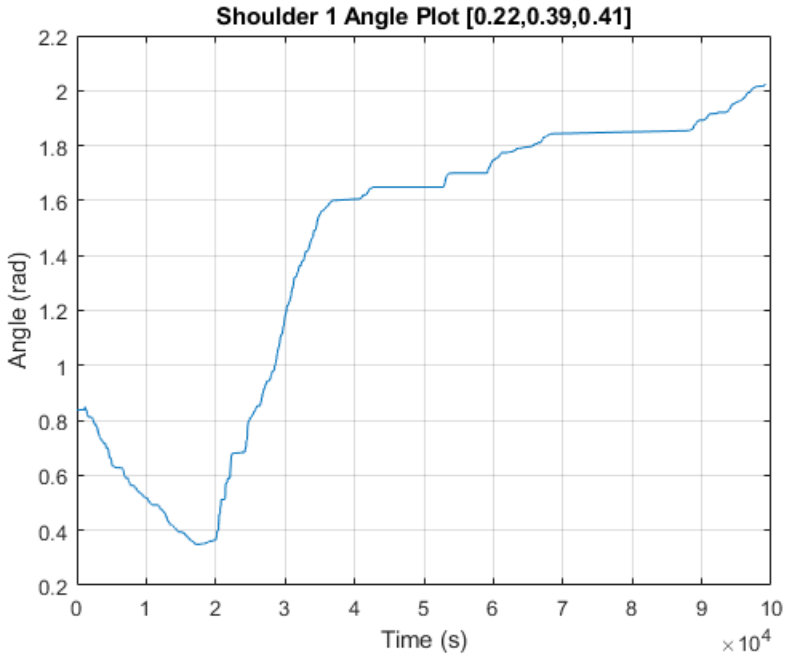
Shoulder 1 Angle Plot [0.22,0.39,0.41]
Angle (rad)
Time (s)
×10^4

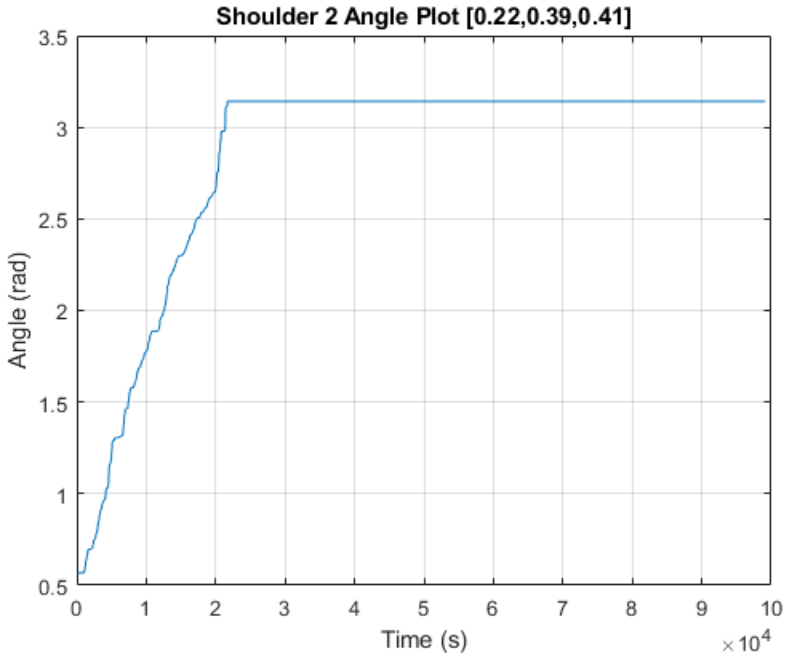
Shoulder 2 Angle Plot [0.22,0.39,0.41]
Angle (rad)
Time (s)
×10^4

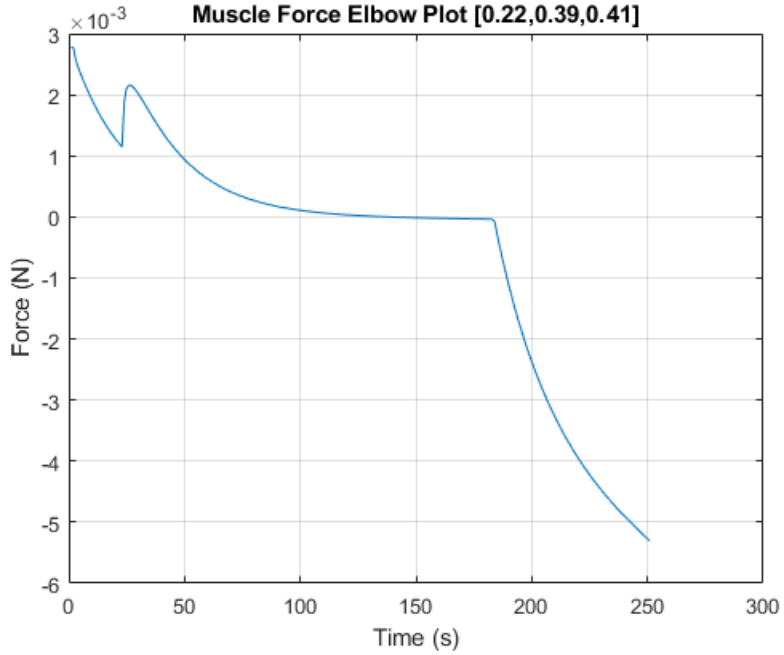
Muscle Force Elbow Plot [0.22,0.39,0.41]
×10^-3
3
2
1
0
-1
-2
-3
-4
-5
-6
Force (N)
0
50
100
150
200
250
300
Time (s)

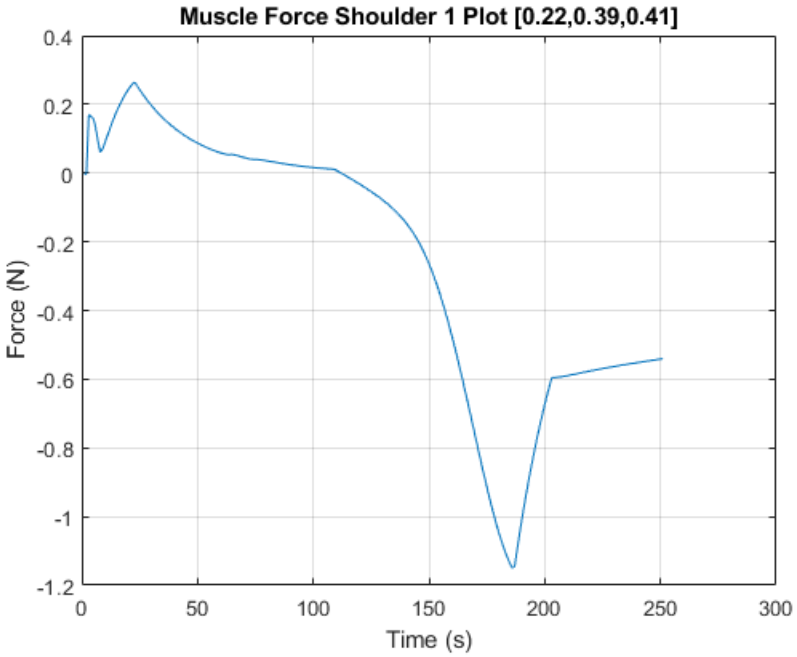
Muscle Force Shoulder 1 Plot [0.22,0.39,0.41]
0.4
0.2
0
-0.2
-0.4
-0.6
-0.8
-1
-1.2
Force (N)
0
50
100
150
200
250
300
Time (s)

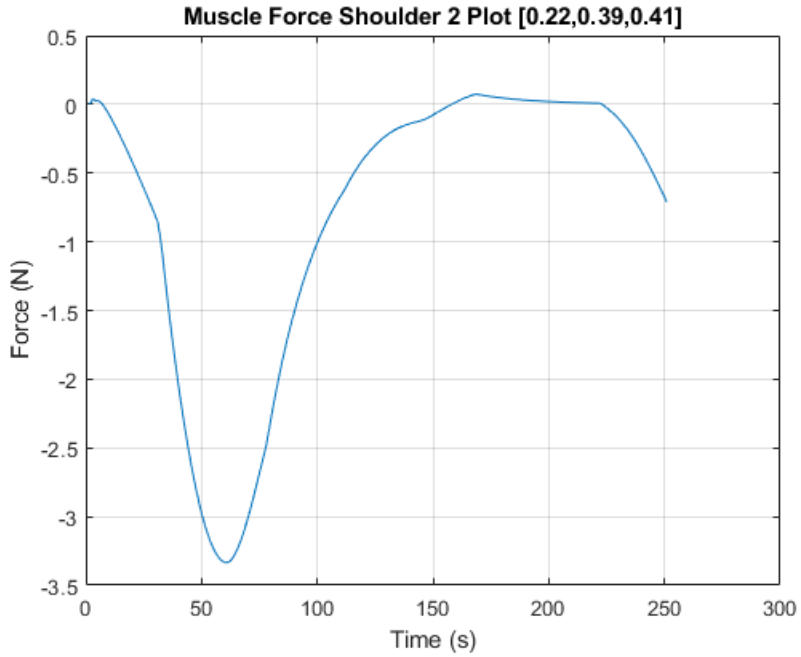
Muscle Force Shoulder 2 Plot [0.22,0.39,0.41]
Force (N)
Time (s)
0.5
0
-0.5
-1
-1.5
-2
-2.5
-3
-3.5
0
50
100
150
200
250
300

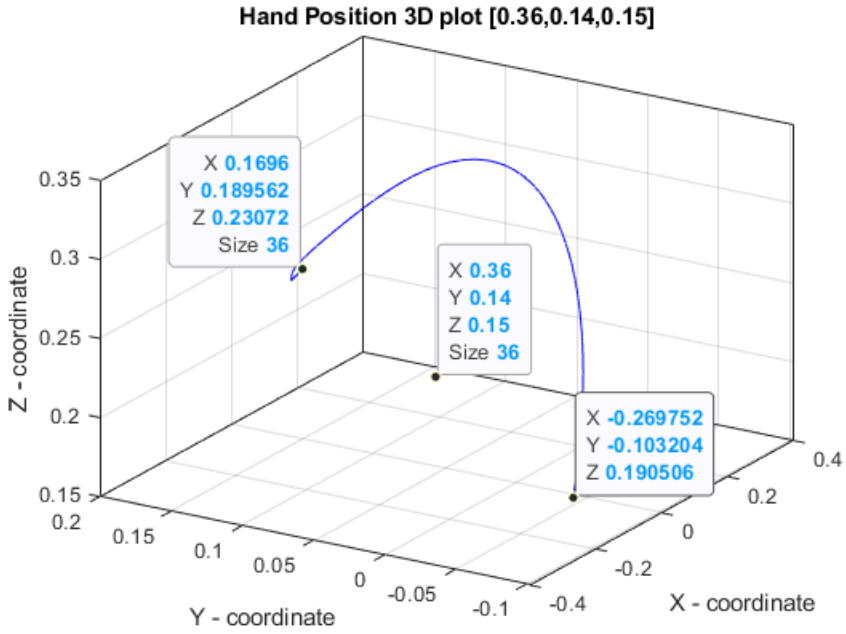
Hand Position 3D plot [0.36,0.14,0.15]
X 0.1696
Y 0.189562
Z 0.23072
Size 36
X 0.36
Y 0.14
Z 0.15
Size 36
X -0.269752
Y -0.103204
Z 0.190506
Z - coordinate
Y - coordinate
X - coordinate

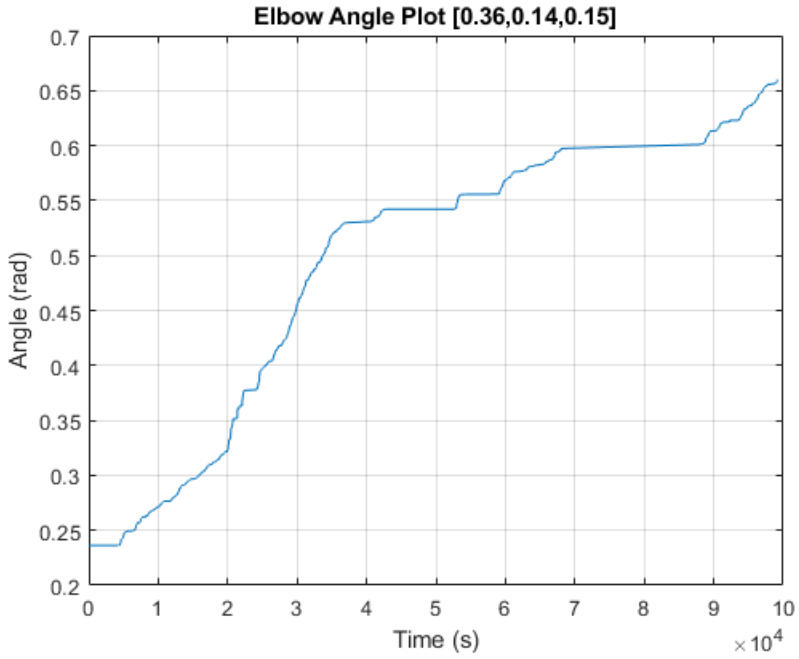
Elbow Angle Plot [0.36,0.14,0.15]
Angle (rad)
Time (s)
×10^4
0.7
0.65
0.6
0.55
0.5
0.45
0.4
0.35
0.3
0.25
0.2
0
1
2
3
4
5
6
7
8
9
10

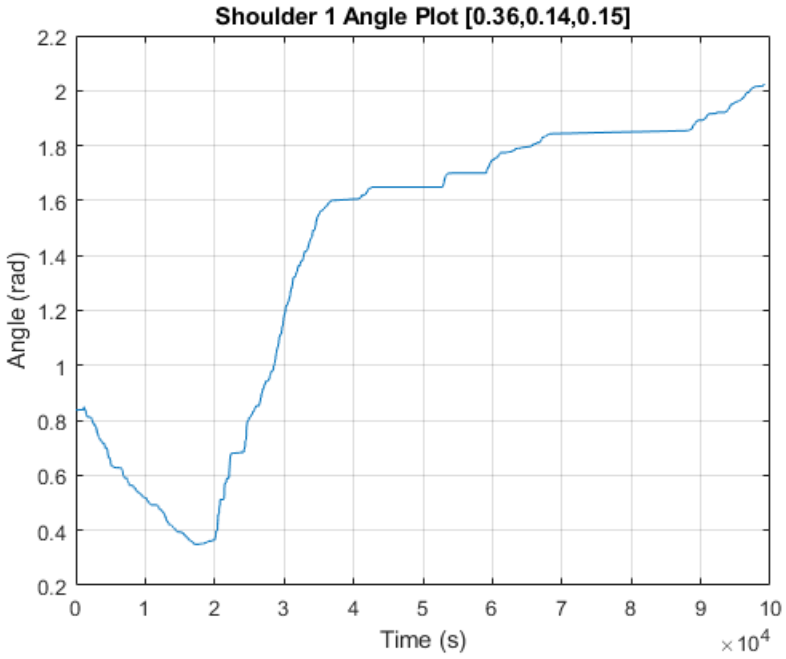
Shoulder 1 Angle Plot [0.36,0.14,0.15]
Angle (rad)
Time (s)
×10^4
2.2
2
1.8
1.6
1.4
1.2
1
0.8
0.6
0.4
0.2
0
1
2
3
4
5
6
7
8
9
10

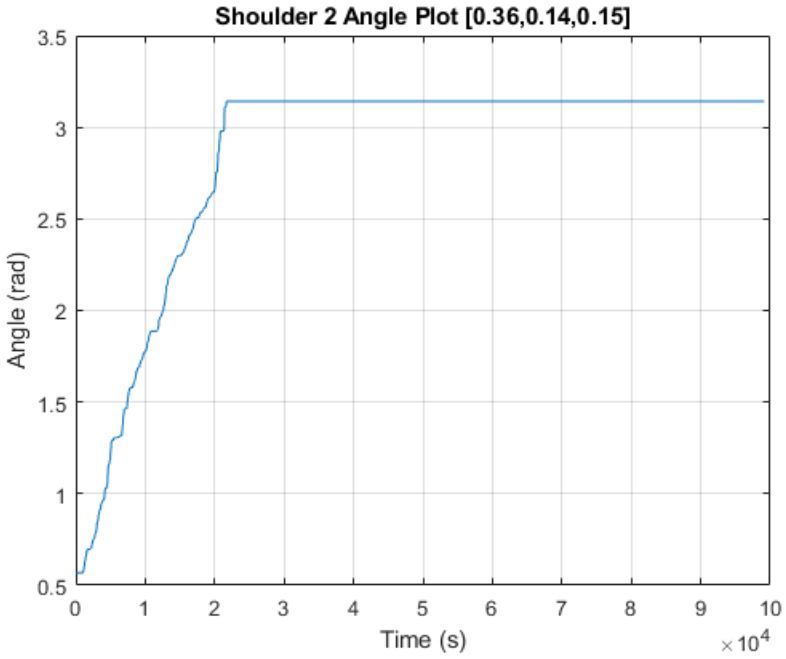
Shoulder 2 Angle Plot [0.36,0.14,0.15]
Angle (rad)
Time (s)
×10^4
3.5
3
2.5
2
1.5
1
0.5
0
1
2
3
4
5
6
7
8
9
10

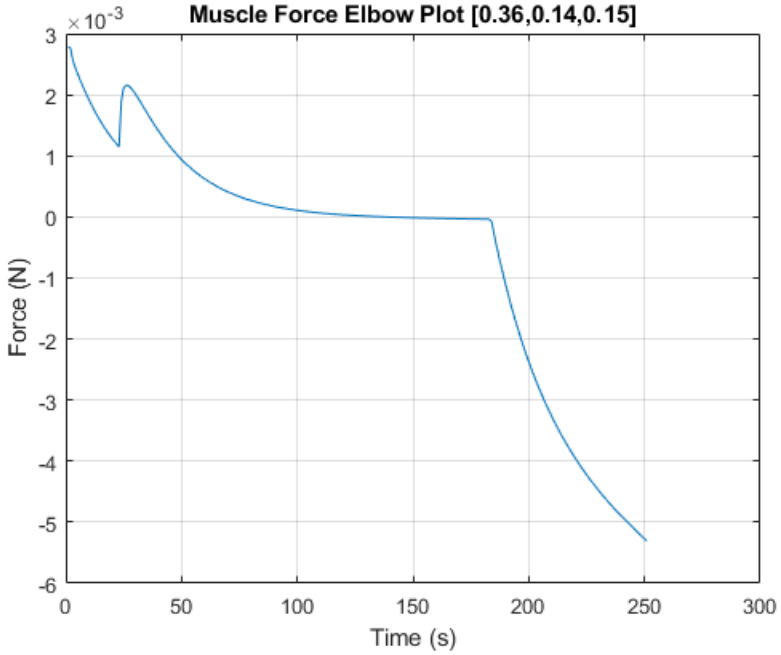
Muscle Force Elbow Plot [0.36,0.14,0.15]
×10^-3
Force (N)
Time (s)
3
2
1
0
-1
-2
-3
-4
-5
-6
0
50
100
150
200
250
300

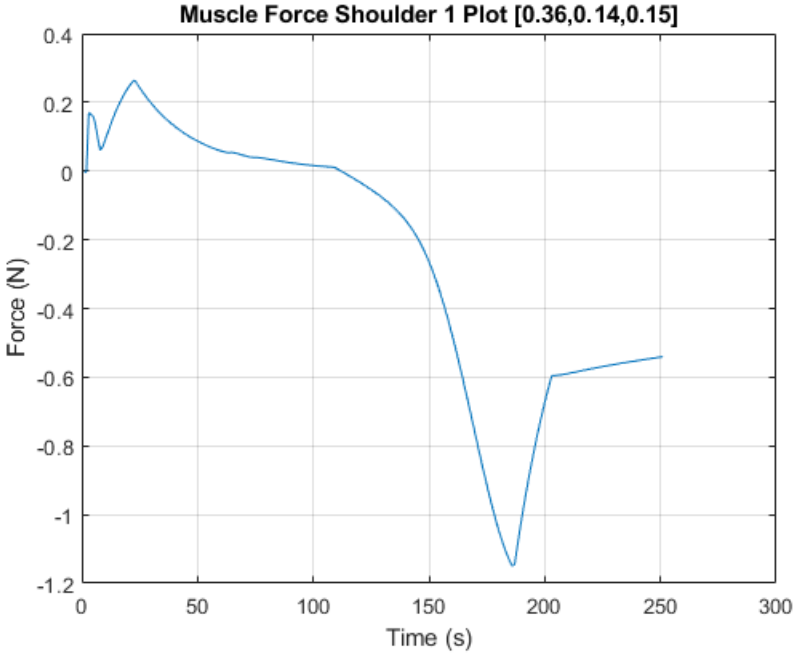
Muscle Force Shoulder 1 Plot [0.36,0.14,0.15]
Force (N)
Time (s)
0.4
0.2
0
-0.2
-0.4
-0.6
-0.8
-1
-1.2
0
50
100
150
200
250
300

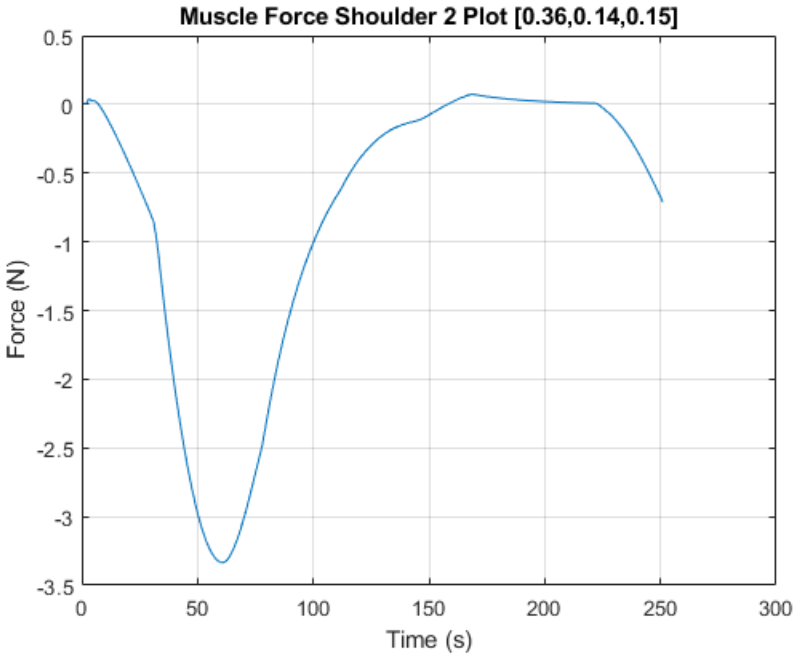
Muscle Force Shoulder 2 Plot [0.36,0.14,0.15]
Force (N)
Time (s)
0.5
0
-0.5
-1
-1.5
-2
-2.5
-3
-3.5
0
50
100
150
200
250
300

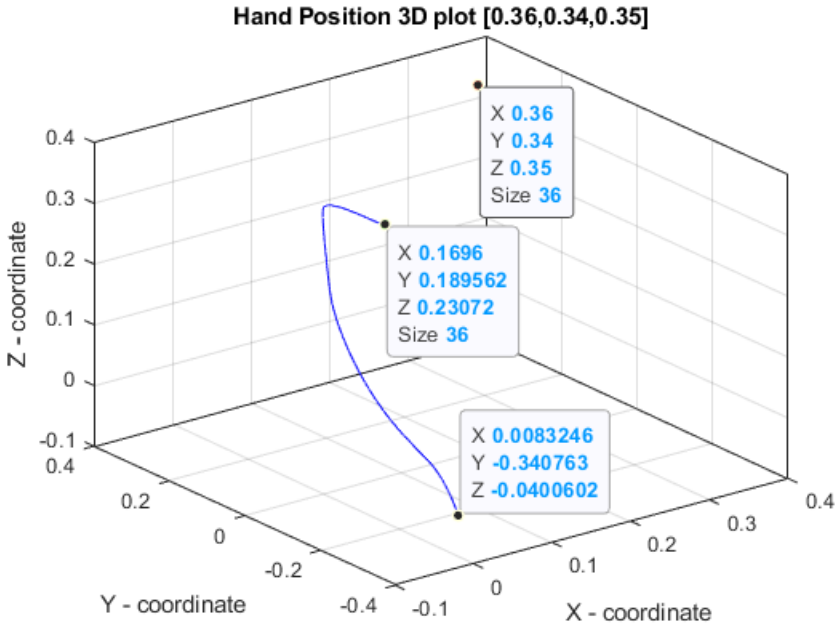
Hand Position 3D plot [0.36,0.34,0.35]
X 0.36
Y 0.34
Z 0.35
Size 36
X 0.1696
Y 0.189562
Z 0.23072
Size 36
X 0.0083246
Y -0.340763
Z -0.0400602
Z - coordinate
Y - coordinate
X - coordinate

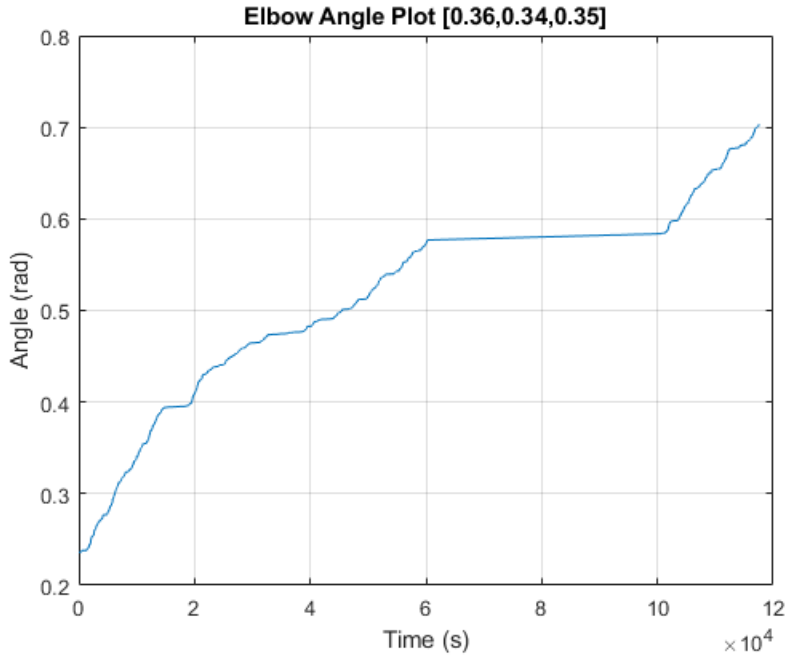
Elbow Angle Plot [0.36,0.34,0.35]
Angle (rad)
Time (s)
×10^4

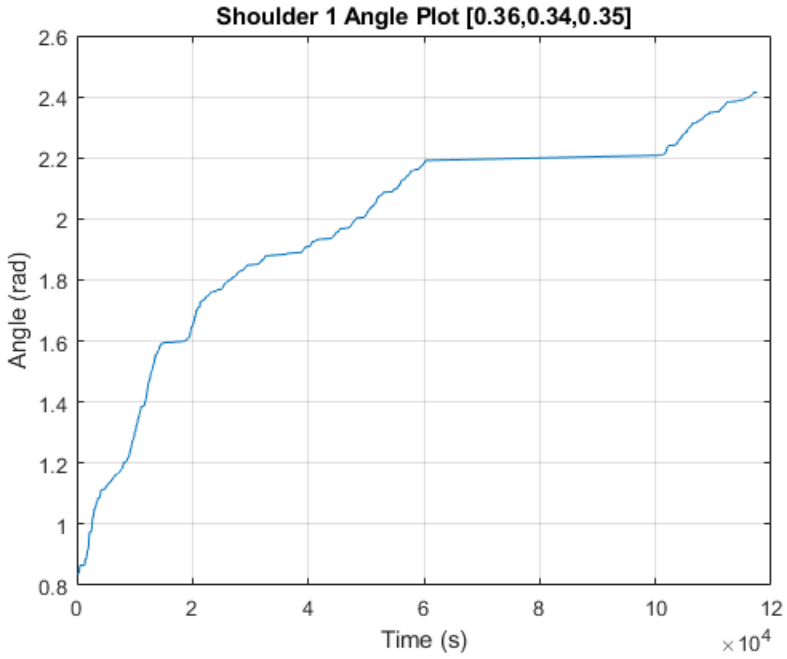
Shoulder 1 Angle Plot [0.36,0.34,0.35]
Angle (rad)
Time (s)
×10^4
2.6
2.4
2.2
2
1.8
1.6
1.4
1.2
1
0.8
0
2
4
6
8
10
12

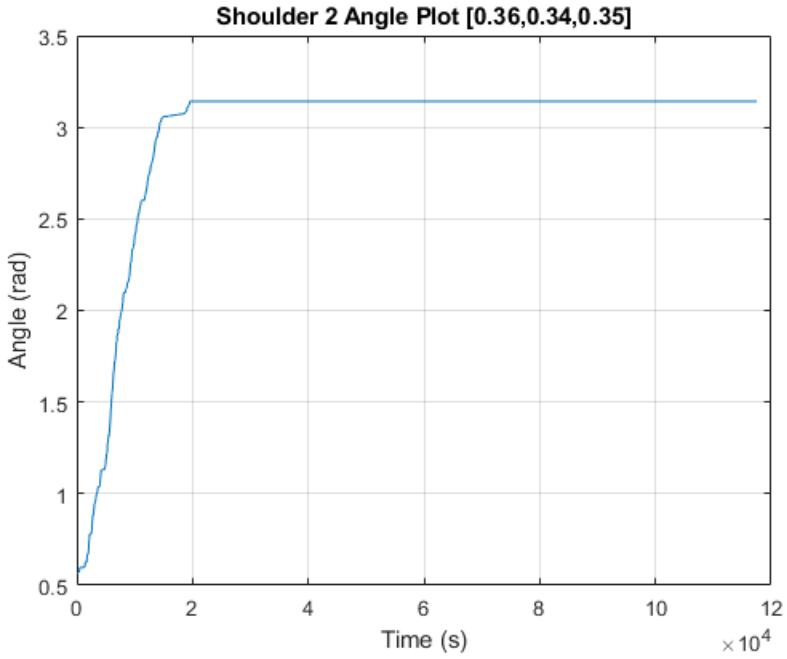
Shoulder 2 Angle Plot [0.36,0.34,0.35]
Angle (rad)
Time (s)
×10^4
3.5
3
2.5
2
1.5
1
0.5
0
2
4
6
8
10
12

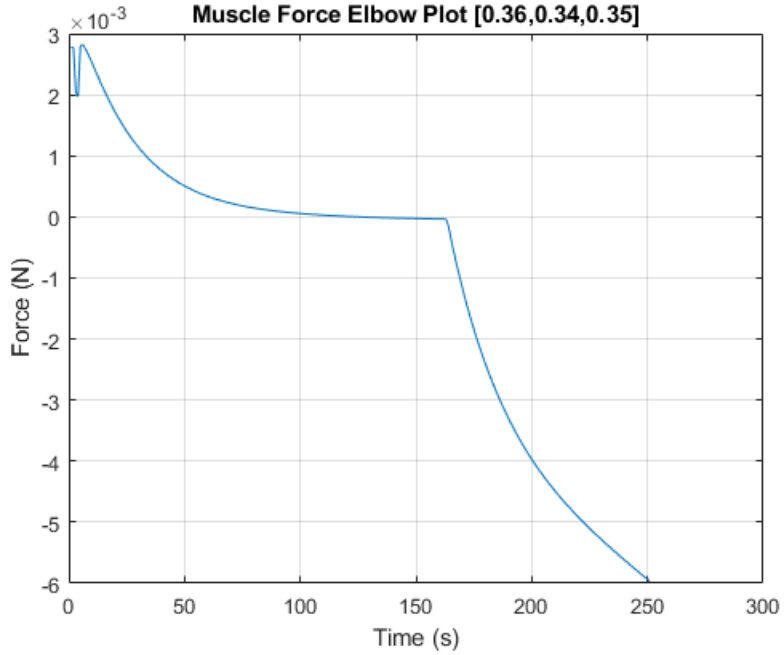
Muscle Force Elbow Plot [0.36,0.34,0.35]
×10^-3
3
2
1
0
-1
-2
-3
-4
-5
-6
Force (N)
0
50
100
150
200
250
300
Time (s)

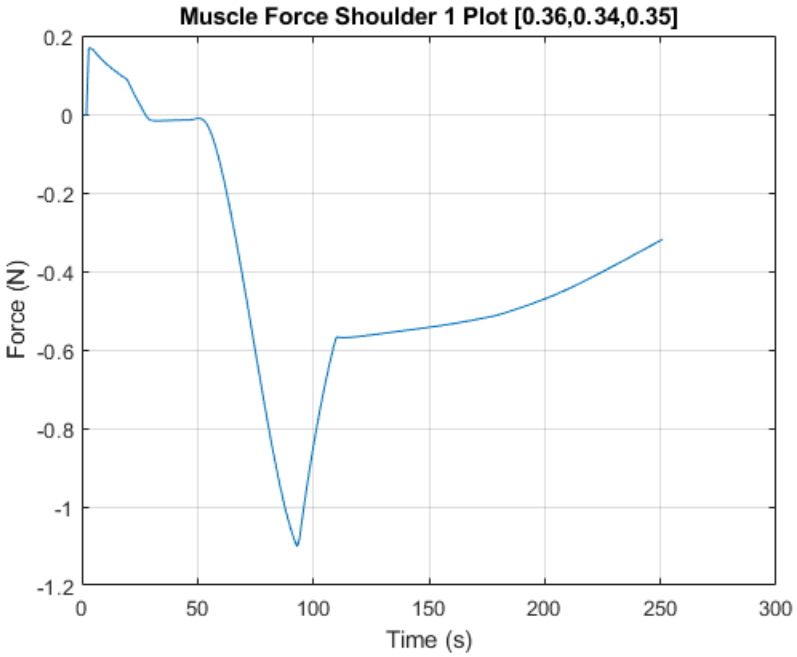
Muscle Force Shoulder 1 Plot [0.36,0.34,0.35]
0.2
0
-0.2
-0.4
-0.6
-0.8
-1
-1.2
Force (N)
0
50
100
150
200
250
300
Time (s)

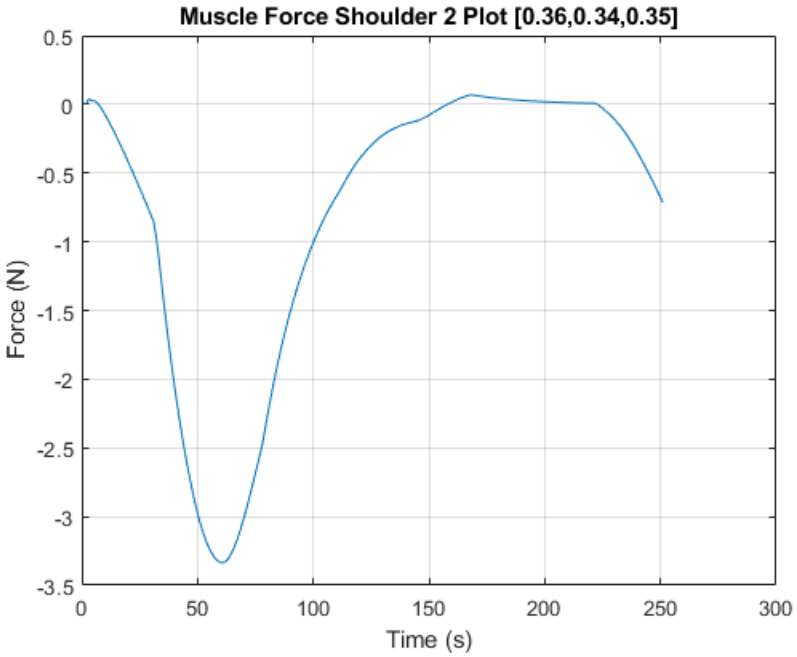
Muscle Force Shoulder 2 Plot [0.36,0.34,0.35]
Force (N)
Time (s)
0.5
0
-0.5
-1
-1.5
-2
-2.5
-3
-3.5
0
50
100
150
200
250
300